6
UWB MIMO Antenna

The rapid growth in wireless communication forces the regulatory authorities to allow the transmission in wider frequency spectrum in order to achieve high wireless channel capacity. It is achieved by using the diversity/multiple-input-multiple-output (MIMO) technology in rich scattering environment without any additional power or spectrum. MIMO technology uses multiple antennas at the transmitter and receiver terminals of the transmission system. The UWB system is also susceptible to multipath fading problems similar to other wireless communication systems. The use of MIMO technology helps to overcome multipath fading and improves the diversity gain [Wallace and Jensen, 2001; Ben *et al*., 2012]. UWB MIMO technology requires high isolation among antenna elements to combat multipath fading. However, the compact UWB MIMO antenna for portable applications in a given smaller area causes the degradation in diversity performance due to presence of various mutual coupling among the antenna elements. In addition, UWB system faces the severe interference challenges with existing narrowband technologies such as WLAN (5.15-5.825 GHz), which lies in the UWB spectrum. Hence, the design of a compact UWB MIMO antenna with band notch characteristics is essential. The aim of this chapter is to investigate the application of fractal geometry in UWB MIMO antenna design with enhanced antenna characteristics.

6.1 Introduction

The UWB technology is growing very rapidly because of its high data transmission capacity in a wide frequency band at very low power level. However, UWB system faces multipath fading challenges in the communication channel because of reflections and diffractions of signals between receiver and transmitter [Foschini and Gans, 1998]. Thus, in order to realize the high data transmission capacity as well as to overcome the multipath fading for short distance communication, MIMO technology is combined with ultrawideband (UWB) technology [Najam *et al.*, 2011; Bolin *et al.*, 2005]. MIMO systems use multiple antennas to transmit and receive signals with different fading characteristics, which help to enhance the system reliability and channel capacity [Rajagopalan *et al.*, 2007; Ben *et al.*, 2012]. During the past few years, several UWB MIMO antennas have been proposed to achieve the wideband isolation, compact size and filtering of interfering bands [Hong *et al.*, 2008; See and Chen, 2009; Zhang *et al.*, 2009; Li *et al.*, 2011; Kelly *et al.*, 2011; Jiangand and Che, 2012; Peng *et al.*, 2014; Lee *et al.*, 2012]. However, the use of multiple antennas in a given smaller area degraded the antenna characteristics because of several mutual couplings. In [See and Chen, 2009; Zhang *et al.*, 2009], the decoupling structures are placed between monopoles to enhance the isolation.

The UWB system faces electromagnetic (EM) interference problems with existing narrowband communication systems such as IEEE 802.11 WLAN from 5.15-5.85 GHz, which operates in the UWB spectrum. To achieve WLAN band rejection in the UWB range, different strips/slots are introduced either in the radiator portion or in the ground plane of the UWB antenna. Some of these are split-ring resonators [Li *et al.*, 2011], open loop resonators [Kelly *et al.*, 2011], and U-shaped structures [Jiangand and Che, 2012]. However, the application of these structures to achieve band rejection could cause additional mutual coupling between the radiating structures. The UWB MIMO antennas with band rejection in WLAN band are

reported in [Peng *et al.*, 2014; Lee *et al.*, 2012]. In [Li *et al.*, 2013; Lihong *et al.*, 2014], compact UWB MIMO antennas are reported in the literature. Moreover, these antennas with acceptable isolation are difficult to integrate with modern portable UWB systems because of their larger dimensions. However, the majorities of these antennas [Ben *et al.*, 2012; Zhang *et al.*, 2009; Li *et al.*, 2011; Kelly *et al.*, 2011; Jiangand and Che, 2012; Peng *et al.*, 2014; Lee *et al.*, 2012] are 2×2 UWB MIMO antenna and did not enhance the quality of the communication channel significantly. In order to increase the channel capacity more number of antennas is required [Karaboikis *et al.*, 2008]. On the other hand, 4×4 UWB MIMO antennas are reported in [Kiem *et al.*, 2014; Mao and Chu, 2014]. The dimensions of the antenna presented in [Kiem *et al.*, 2014] are very large, whereas [Mao and Chu, 2014] does not have the band reject characteristics. Hence, the design of a compact UWB MIMO antenna with band rejection and low mutual coupling in a given smaller area for portable electronic devices is very challenging task.

The application of fractal geometry in antenna design provides desired miniaturization and wideband phenomena because of its self-similarity and space filling properties [Werner *et al.*, 1999; Anguera *et al.*, 2005; Hashemi *et al.*, 2006]. The space filling property helps to increases the effective electrical path length of the antenna in a given small area [Werner *et al.*, 1999; Anguera *et al.*, 2005]. This implies that use of fractal geometry provide increment in electrical path length in a smaller area. A number of fractal geometries, for example, Koch snowflake [Anguera *et al.*, 2005], hexagonal shaped [Werner *et al.*, 1999], and Sierpinski triangle [Werner *et al.*, 1999; Anguera *et al.*, 2005] are used to design UWB antenna. The application of fractal geometry in antenna design also helps to stabilize the radiation pattern at higher frequencies [Fereidoony *et al.*, 2012].

6.2 Circular UWB MIMO Antenna with Fractal Ground Slot

6.2.1 Antenna Design

(a) Antenna Configuration

The geometry of the proposed UWB MIMO antenna (UMA) is shown in Figure 6.1. The antenna is fabricated on FR4 substrate with dimensions of 25 mm × 35 mm × 1.6 mm, dielectric constant of 4.4, and loss tangent of 0.02. Two circular monopoles (CMs) are placed orthogonal to each other for good isolation between the antenna elements [Karaboikis *et al.*, 2008]. The CM1 and CM2 of MIMO antenna with their respective 50 Ω microstrip feed lines are printed on one side of the substrate, whereas ground plane is printed on the other side. Both the monopoles are identical with a dimension of radius R. The wideband isolation of better than 16 dB is achieved by an L-shaped structure that extends from ground plane. It is demonstrated that by etching rectangular slot [Zaker *et al.*, 2008; Amiri *et al.*, 2012] and L-shaped slot [Zaker *et al.*, 2009] in the ground plane; fractional bandwidth up to 125% is achieved.

Therefore, a fractal slot generated using Minkowski fractal geometry is introduced in the ground plane, below the feed line. The fractal slot helps to achieve the wideband phenomena as well as stable radiation pattern at higher frequencies [Fereidoony *et al.*, 2012]. The iteration wise generation of the Minkowski fractal slot is shown in Figure 6.2. The band rejection in WLAN band is achieved by etching ESRR shaped slot from each CMs. These ESRR shaped slots are similar to monopoles and used to provide the narrower and stronger notch-bands [Zhang *et al.*, 2008]. Moreover, the use of ESRR provides miniaturization in band notch structures, because an ellipse possesses greater area than the circle. The design and optimization of antenna is carried out using Ansoft HFSS v.13. The optimized dimensions of the antenna are as: L = 25 mm, W = 35 mm, R = 5 mm, W_m = 2.5 mm, L_g = 8 mm, d = 0.6 mm, h = 2.4 mm, w = 0.3 mm, L_1 = 1 mm, L_2 = 16 mm, L_3 = 1 mm, L_3 = 8 mm, W_1 = 5 mm, W_2 = 7.25 mm, W_3 = 13.5 mm, L_{s1} = 2 mm, W_{s1} = 9 mm, L_{s2} = 2.5 mm, L_{ma} = 6.4 mm and L_{mi} = 4 mm.

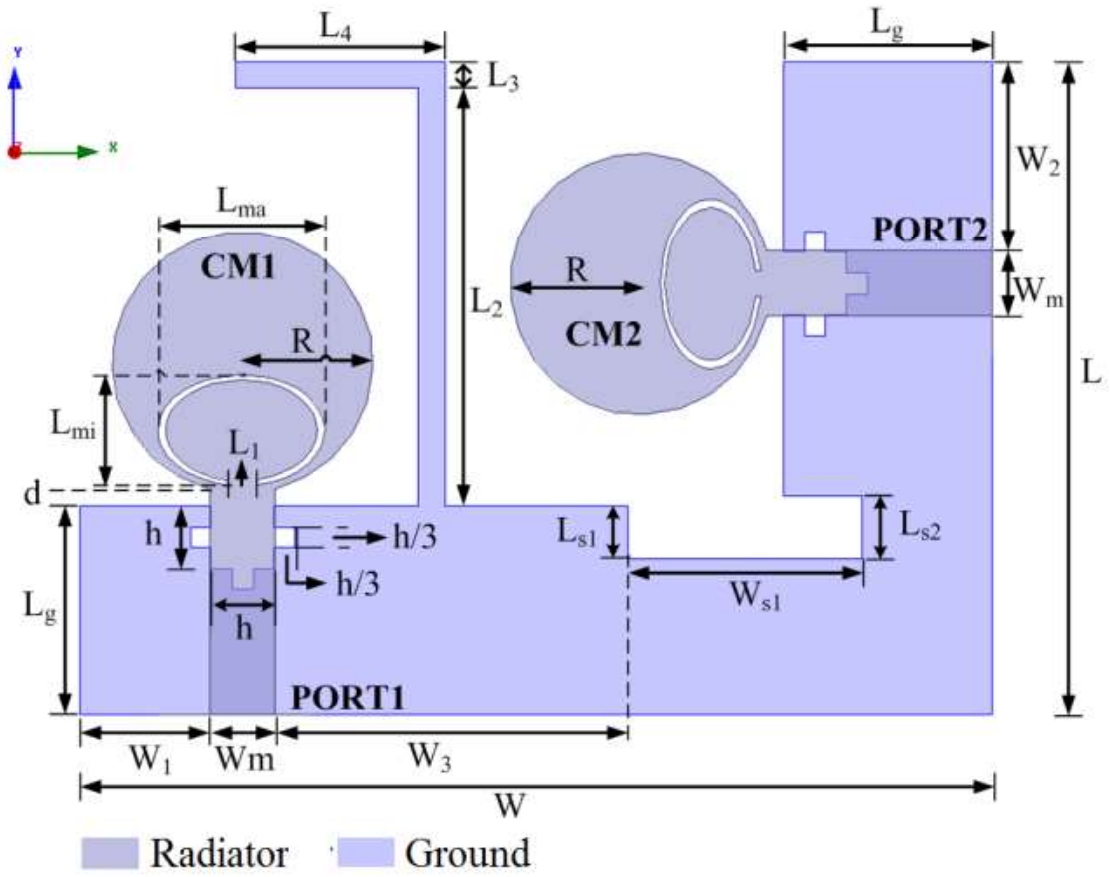

Figure 6.1: The optimized geometry of the proposed UWB MIMO antenna

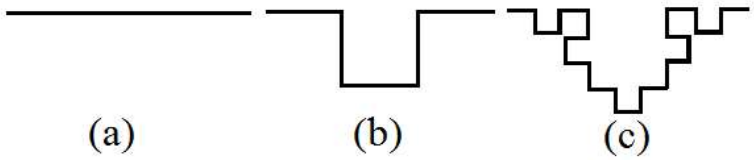

Figure 6.2: The iterative generation of the Minkowski fractal slot (a) Iteration-0, (b) Iteration-1 and (c) Iteration-2

(b) Effect of L-shaped ground stub

In order to achieve wideband isolation, an L-shaped stub is protruded from the ground plane of UWB MIMO antenna. It works as a reflector that improves the isolation by separating the CMs radiation patterns. The effect of stub on S-parameters is displayed in Figure 6.3. It is observed from Figure 6.3(a) that after the introduction of L-shaped stub S_{11} performance at lower UWB frequencies improve significantly, whereas S_{22} shows slight improvement in the higher UWB frequency range. In Figure 6.3(b), with the grounded stub, one can see the improvement in isolation at lower as well as at higher operating frequencies, which helps to achieve the better isolation (>16 dB) between CMs in the entire UWB band.

To further investigate the effect of L-shaped stub, surface current distributions of the UMA at 4.1 GHz resonant frequency is shown in Figure 6.4. It can be seen that the flow of surface current from port1 to port2 has been reduced due to strong coupling of surface current with the grounded stub. This helps to enhance the isolation between the CMs.

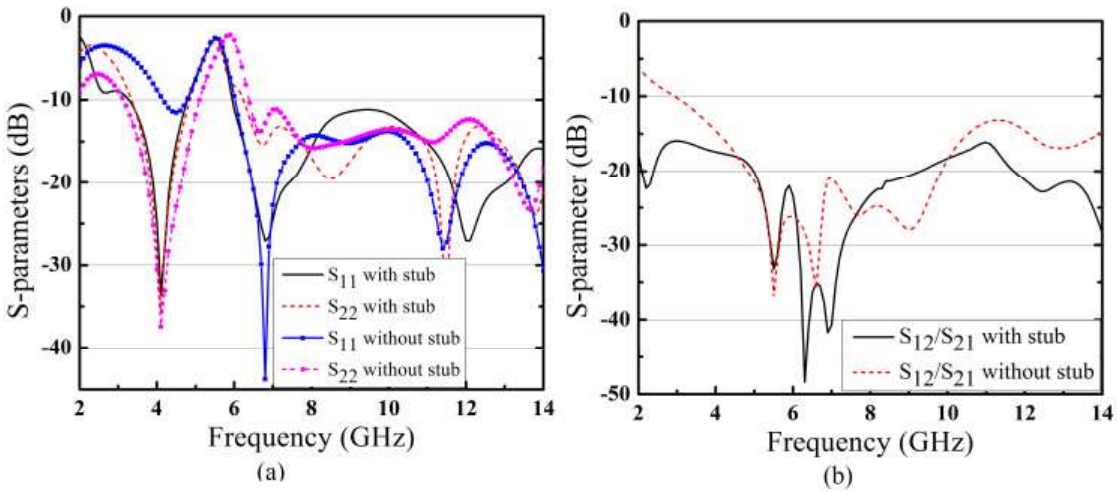

Figure 6.3: Simulated S-parameters variation of proposed fractal UWB MIMO antenna with and without ground stub (a) S_{11} and S_{22}, (b) S_{12}/S_{21}

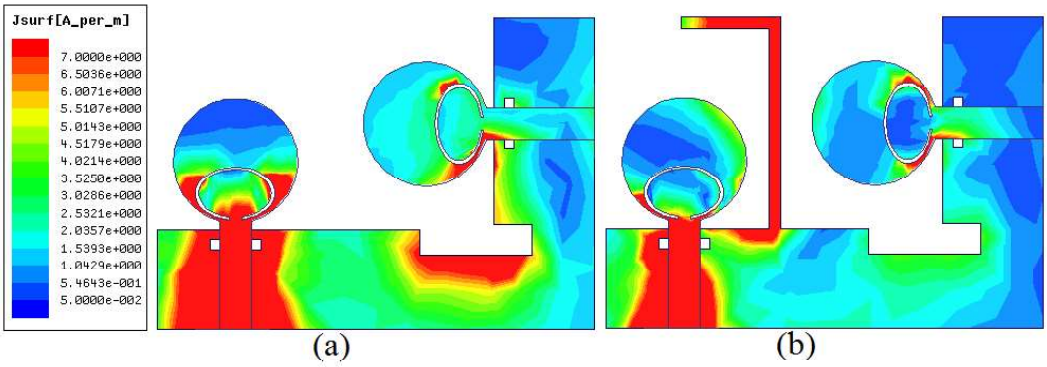

Figure 6.4: Simulated surface current distribution when port1 is excited at 4.1 GHz (a) without L-shape stub (b) with L-shape stub

(c) Effect of Elliptical Split-Ring Resonator (ESRR)

In this study, an ESRR slot is etched from each CM to achieve the band rejection at 5.5 GHz WLAN band (5.15-5.85 GHz). The notch length (L_n) of an ESRR slot of major axis length (L_{ma}), minor axis length (L_{mi}) and width (w) is calculated using following mathematical formula:

$$L_n = K\pi(0.5L_{mi} - w) \approx \frac{\lambda_g}{2} \approx \frac{c}{2f_{notch}\sqrt{\varepsilon_{eff}}} \tag{6.1}$$

$$K = 3(1+k) - \sqrt{(3+k)(1+3k)} \tag{6.2}$$

$$k = \frac{L_{ma}}{L_{mi}} \tag{6.3}$$

where, c is speed of the light, λ_g is guided wavelength, ε_{eff} is the effective dielectric constant as calculated in [Pozar, 1998], K and k are ellipse circumference parameters [Bourke, 2013]. The calculated length L_n of the ESRR slot using Eq. (6.1) is found to be 13.01 mm, whereas actual

length is 14.06 mm, which is close to calculated length. Figure 6.5 shows the simulated surface current distributions of the UMA at 5.5 GHz. It is observed that intensity of surface current at inner and outer edges of ESRR is very strong, when port1/port2 is excited. This causes for the suppression of radiation characteristics of the UMA at 5.5 GHz notch band.

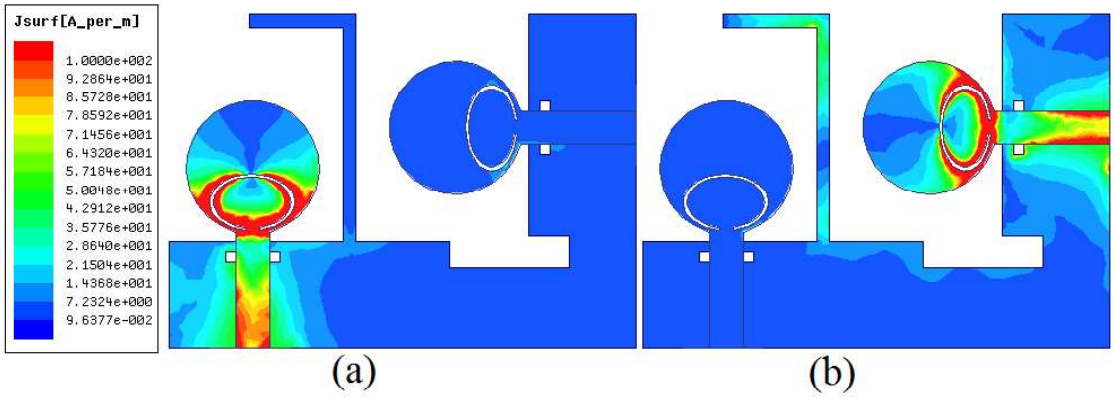

Figure 6.5: Simulated surface current distribution at 5.5 GHz band notch frequency (a) port 1 is excited, (b) port 2 is excited

6.2.2 Results and Discussion

(a) S-parameter Result

The presented UMA is fabricated to verify the feasibility of the prototype and measurement is performed by the Agilent E5071C VNA. The photograph of fabricated prototype is shown in Figure 6.6. Figure 6.7 shows the measured and simulated S-parameters. It can be seen from Figure 6.7(a) that measured S_{11} response is 2.6-13.5 GHz, whereas S_{22} response is from 3.4-14 GHz, excluding WLAN band in both the cases. Some discrepancies are observed due to soldering, SMA connectors and fabrication tolerances. It is seen from Figure 6.7(b) that the isolation of more than 16 dB is observed in the entire UWB band. This shows the good agreement with simulated results.

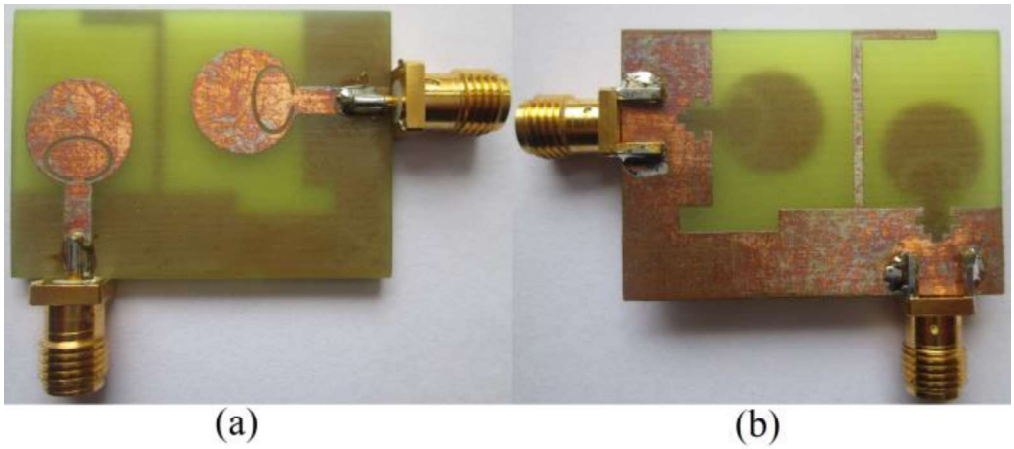

Figure 6.6: Fabricated prototype of the proposed UMA (a) front view and (b) Bottom view

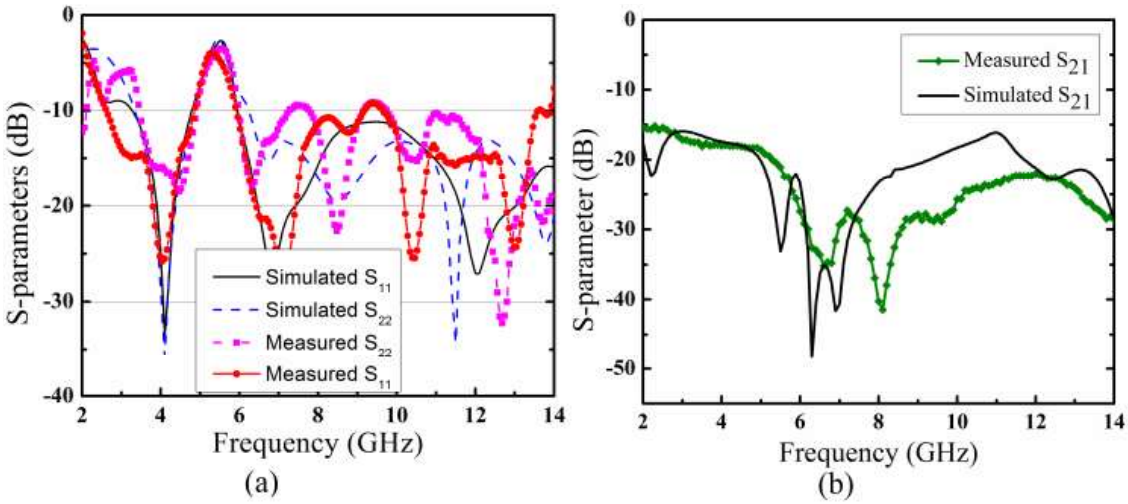

Figure 6.7: Comparison of Measured and Simulated S-parameters (a) S_{11} and S_{22}, and (b) S_{21}/S_{12}

(b) Radiation Performance

The measured gain of the proposed antenna for both ports in the UWB band is shown in Figure 6.8. When port 1 is excited then port 2 is matched with 50Ω load, and vice versa. The gain response variation of the antennas is within 3dB range, excluding WLAN notch band, and suppressed significantly in the notch band. The radiation pattern of the UMA at 4.1, 6.8 and 12 GHz resonant frequencies in E-plane (*xz*-plane) and H-plane (*yz*-plane) are shown in Figure 6.9. It is observed that E-plane pattern is nearly symmetrical. Moreover, H-plane pattern at lower resonant frequencies are almost similar to each other. During the measurement, when port1 is excited than port2 is matched by a 50 Ω load, and vice versa. However, radiation pattern at higher resonant frequencies is distorted compared to lower resonant frequencies due to change in current nature from standing wave at lower resonant frequencies to travelling wave at higher resonant frequencies.

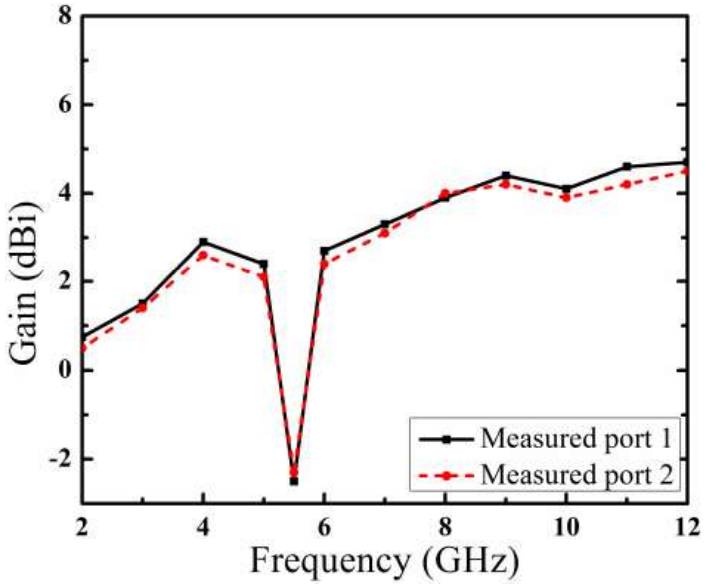

Figure 6.8: Measured gain of the proposed UWB MIMO antenna

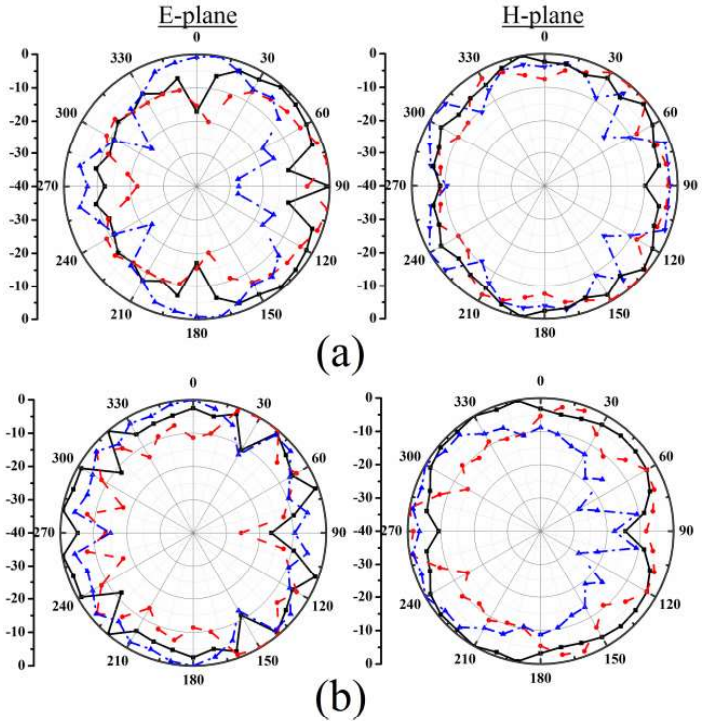

Figure 6.9: Radiation characteristics of the UWB MIMO antenna in E-plane and H-plane at 4.1 GHz (——), 6.8 GHz (– –) and 12 GHz (—·—·—) (a) port 1 is matched, (b) port 2 is matched

(c) Diversity Performance

The envelope correlation coefficient (ECC) is an important constraint to analyze the diversity characteristics of a MIMO antenna and calculated using S-parameters [Fereidoony *et al.*, 2012]:

$$\rho_e = \frac{\left|S_{11}^* S_{12} + S_{21}^* S_{22}\right|^2}{(1-(|S_{11}|^2+|S_{21}|^2))(1-(|S_{22}|^2+|S_{12}|^2))} \tag{6.4}$$

The ECC of the proposed UMA has shown in Figure 6.10. It is observed that its value is less than 0.01 within entire UWB band because of efficient design of the presented antenna. Moreover, for good diversity performance its threshold value should be less than 0.5 [Karaboikis *et al.*, 2008]. Similarly, the quality of UWB MIMO system in a rich multipath environment is estimated in terms of capacity loss (b/s/Hz) also. In a communication channel, this parameter is used to define the upper bound of rate of transmission for reliable transmission. In case of a 2×2 MIMO antenna its threshold value should be less than 0.4 b/s/Hz for reliable transmission [Zhang *et al.*, 2008; Pozar, 1998], and it is estimated mathematically using the correlation matrix as given in [Pozar, 1998], using the equation (5).

$$C_{loss} = -\log_2 \det\left(\psi^R\right) \tag{6.5}$$

where ψ^R is the correlation matrix of the receiving antenna and expressed mathematically as:

$$\psi^R = \begin{bmatrix} \rho_{11} & \rho_{12} \\ \rho_{21} & \rho_{22} \end{bmatrix}, \qquad \rho_{ii} = 1-\left(|S_{ii}|^2+|S_{ij}|^2\right) \qquad \rho_{ij} = -\left(S_{ii}^* S_{ij} + S_{ji}^* S_{ij}\right),$$

for i, j = 1 or 2

The capacity loss changes with the variation of frequencies are shown in Figure 6.10. It can be seen that the capacity loss value are always less than 0.3 b/s/Hz (mostly less than 0.2 b/s/Hz), except WLAN notch band, in the UWB operating range, which is lower than the threshold value 0.4 b/s/Hz.

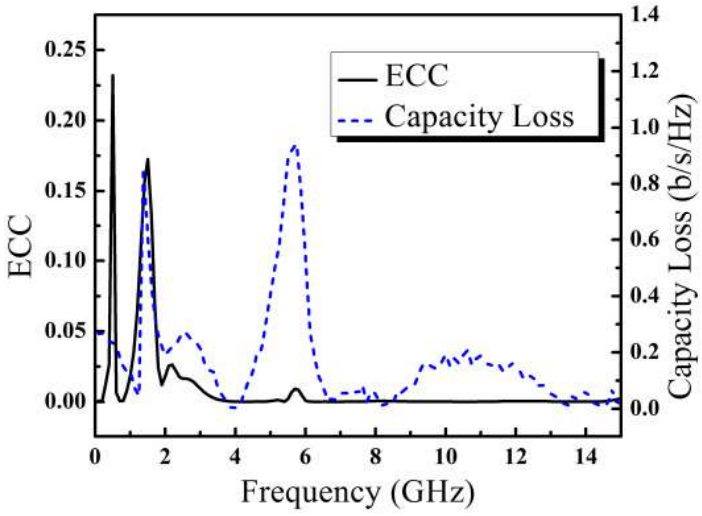

Figure 6.10: ECC and capacity loss of the proposed UWB MIMO antenna

6.3 Fractal Minkowski UWB MIMO Antenna

6.3.1 Antenna Design

(a) Antenna Configuration

The geometry of the Minkowski fractal UWB MIMO antenna with WLAN band notch characteristics is shown in Figure 6.11. It has compact dimensions of 40 mm × 25 mm × 1.6 mm. The presented prototype is fabricated on FR4 substrate, with dielectric constant of 4.4 and loss tangent of 0.02. Both, the octagonal shaped fractal monopoles are identical to each other and placed orthogonally for better isolation. A 50 Ω microstrip line is used to fed both the fractal monopole. The iterative generation of Minkowski fractal geometry is shown in Figure 6.12. The iteration wise application of Minkowski fractal at the edges of Octagonal geometry is presented in Figure 6.13. Here, octagonal shaped geometry work as an initiator and Minkowski geometry work as a generator in the design of monopole of the antenna. To further improve the isolation and enhance the operational bandwidth within a smaller area, one out of eight fractal segment of monopole is etched from the geometry. When both antennas are close to each other, isolation response of the antenna degraded significantly. This modification in geometry increases the separation between orthogonal fractal monopole.

The introduction of rectangular slots in the ground plane helps to achieve the UWB operational bandwidth. An L-shape ground stub is extended from the ground between the two monopoles. The band rejection in WLAN band is obtained by etching C-shape slot from the fractal monopole of the UWB MIMO antenna. The process of analysis and designing of the proposed UWB MIMO antenna is carried out using Ansoft HFSS ver.13. The optimized dimension are: W = 40 mm, R = 4.6 mm, W_m = 2.6 mm, L_g = 8.5 mm, T = 0.3 mm, d = 1mm, L_1 = 1.2 mm, L_2 = 3.4 mm, L_3 = 7 mm, L_4 = 15.5 mm, L_5 = 1 mm, L_6 = 2.5 mm, W_1 = 7mm, W_2 = 8.5 mm, L_{s1} = 2.5 mm, W_{s1} = 2 mm, L_{s2} = 1.5 mm, W_{s2} = 4 mm, L_{s3} = 2 mm, W_{s3} = 10.5 mm, L_{s4} = 3 mm, W_{s4} = 1 mm, L_{s5} = 1.5 mm and W_{s5} = 2 mm.

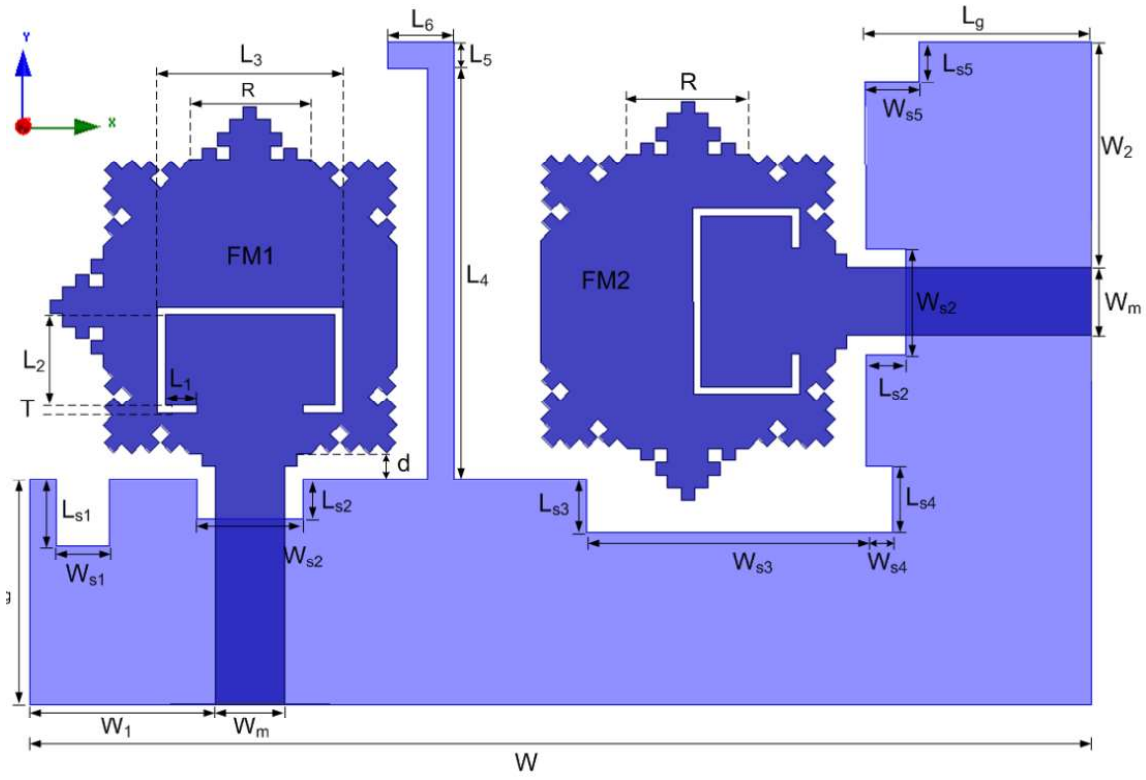

Figure 6.11: Geometry of the proposed fractal UWB MIMO antenna

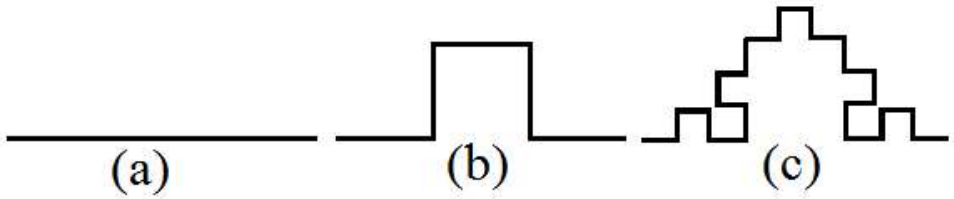

Figure 6.12: Recursive Generation of Minkowski structure (a) Iteration-0, (b) Iteration-1 and (c) Iteration-2

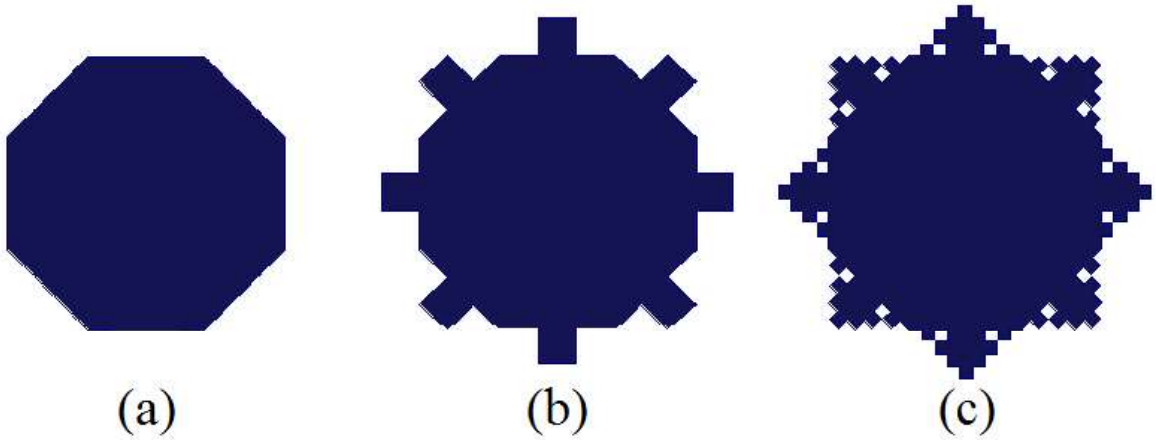

Figure 6.13: Evolution of the fractal monopole of antenna structure with the application of Minkowski geometry at the edges of Octagonal geometry (a) Initiator, (b) After 1st iteration and (c) After 2nd iteration

(b) Effect of L-shaped ground stub

Figure 6.14 shows the effect of ground stub on the s-parameters. It is observed from Figure 6.14(a) that S_{11} response at lower frequency of operating band is reduced as well as improves at higher frequency range when ground stub is present because of increment in the surface current path. Figure 6.14(b) presents the isolation variation of UWB MIMO antenna with and without ground stub. It is observed that S_{21}/S_{12} response is significantly reduced to below -15 dB in the UWB operating range, which in turn helps to achieve decoupling bandwidth in the UWB range.

The effect of stub is better understood using surface current distribution at 4 and 10.2 GHz resonant frequencies as displayed in Figure 6.15. It is observed that when ground stub is not present, surface current is distributed at fractal monopole1 (FM1) and fractal monopole2 (FM2). Moreover, surface current distribution intensity is strong at FM1 compared to FM2. However, mutual coupling is significantly reduced at FM2 after the integration of L-shape ground stub because of strong current associated with the ground stub, which in turn leads to improve the isolation and operational bandwidth.

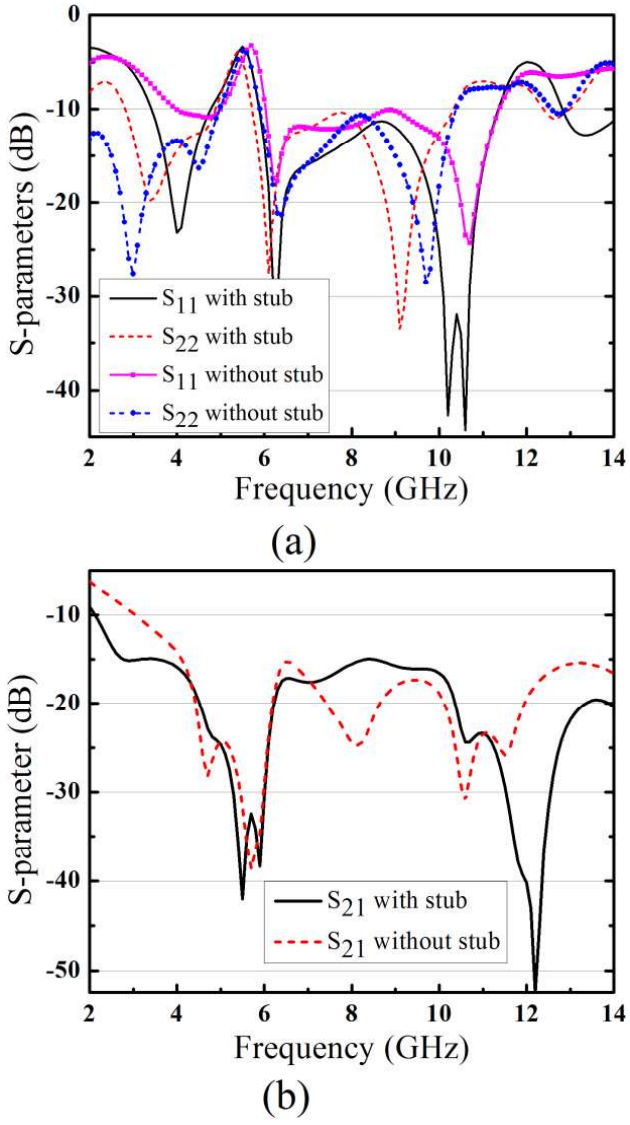

Figure 6.14: Simulated S-parameters variation of proposed fractal UWB MIMO antenna (a) S_{11} and S_{22}, (b) S_{21}/S_{12}

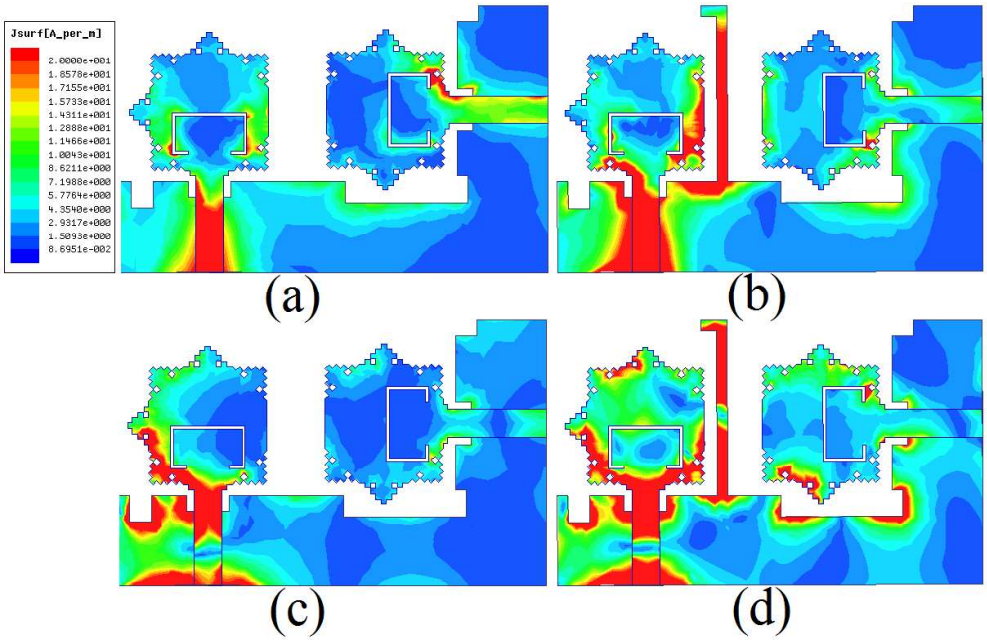

Figure 6.15: Simulated surface current distribution (a) at 4 GHz without L-shape stub (b) at 4 GHz with L-shape stub (c) at 10.2 GHz without L-shape stub (d) at 10.2 GHz with L-shape stub

(c) Effect of C-shape slot

The band notch characteristics at WLAN band is obtained by etching C-shape slot from the fractal monopole of the antenna. The length of the slot is calculated mathematically by-

$$L = \frac{c}{2f_{notch}\sqrt{\varepsilon_{eff}}} \approx 2L_1 + 2L_2 + L_3 \tag{6.6}$$

where, c is speed of light, f_{notch} is center frequency of notch band, ε_{eff} is the effective dielectric constant [Pozar, 1998], and L is the length of the slot.

The simulated surface current distribution of antenna at notch frequency is shown in Figure 6.16. It is observed that current intensity is high at the inner and outer boundaries of C-shape slot. This leads to high attenuation at notch frequency.

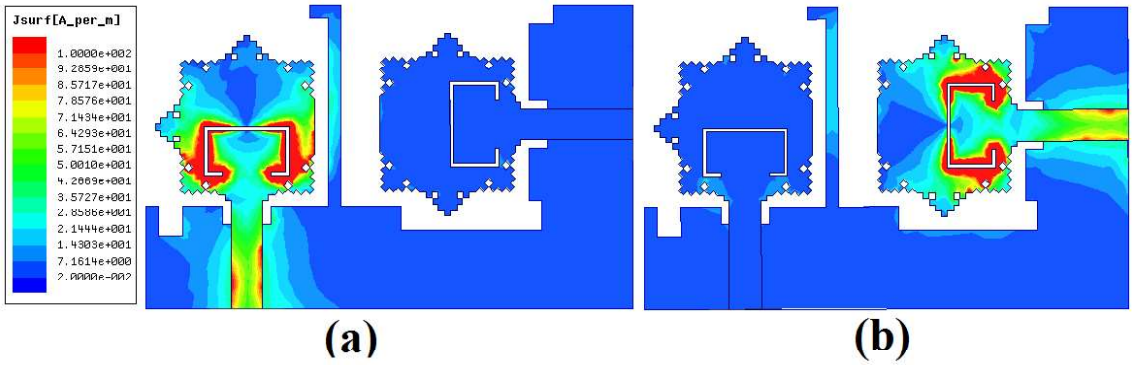

Figure 6.16: Simulated surface current distribution at 5.5 GHz notch frequency (a) with notch structure and (b) without notch structure

6.3.2 Results and Discussion

(a) S-parameter Result

The presented UWB MIMO antenna is fabricated and measurement is performed using Agilent E5071C vector network analyzer (VNA). The photograph of the fabricated UWB antenna top view and bottom view is shown in Figure 6.17. The simulated and measured S_{11}, S_{22} and S_{21} of the UWB MIMO antenna are shown in Figure 6.18. As displayed in Figure 6.18(a), S_{11}<-10dB and S_{22}<-10dB in the UWB operating range, except WLAN notch band, is achieved. The mutual coupling behavior of antenna is less than -15 dB. Thus, the presented UWB MIMO antenna satisfies the desired characteristics in the UWB operating range.

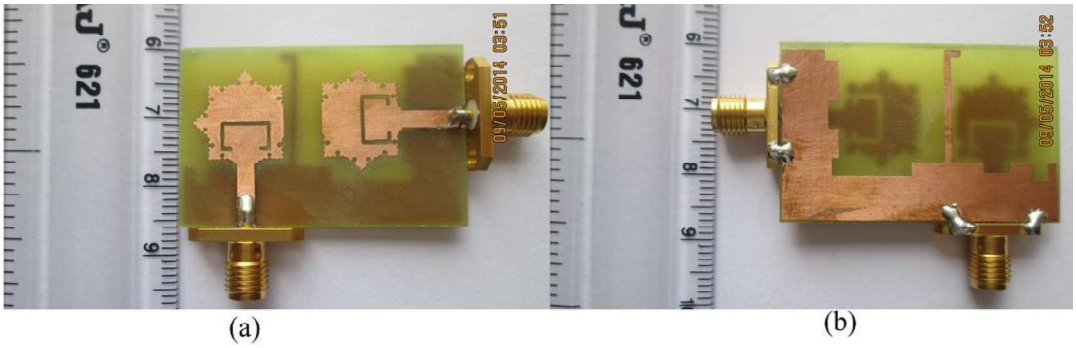

Figure 6.17: Photograph of the fabricated UWB MIMO antenna (a) front view and (b) rear view

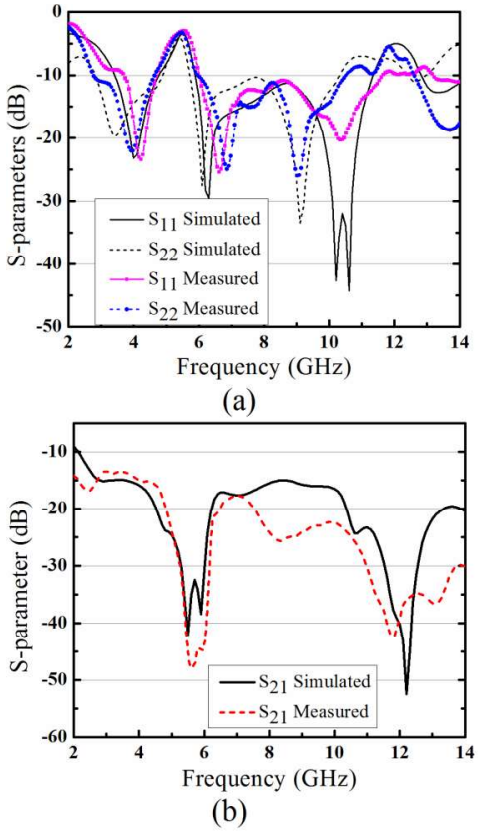

Figure 6.18: Comparison of simulated and measured S-parameters result (a) S_{11} and S_{22}, (b) S_{21}/S_{12}

(b) Radiation Performance

Figure 6.19 shows the measured radiation pattern in E-plane (*yz*-plane) and H-plane (*xz*-plane) at different resonant frequencies. Figure 6.19(a) shows the radiation pattern at resonant frequencies when port 2 is excited and port 1 is matched with a 50Ω load, whereas in case of Figure 6.19(b) port 1 is excited and port 2 is matched with a 50Ω load. It is observed that radiation pattern is nearly quasi-omnidirectional in H-plane. The radiation pattern at higher frequencies shows small distortion compared to lower frequencies due to the reflection at edges from the fractal monopole. The bends and curves of fractal geometry cause for the change in current path, which in turn leads to enhancement in radiation characteristics of the antenna [Balanis, 2005]. The surface current distribution intensity at the fractal edges of the monopole of the antenna is significant at lower and higher resonant frequencies. This helps to improve the antenna gain too. Figure 6.20 shows the measured gain of the proposed antenna for both ports (when port 1 is excited, port 2 is terminated with 50Ω load, and vice versa) in the UWB band. The gain response is within 3dB variation range outside WLAN notch band. The gain response is suppressed significantly in the notch band.

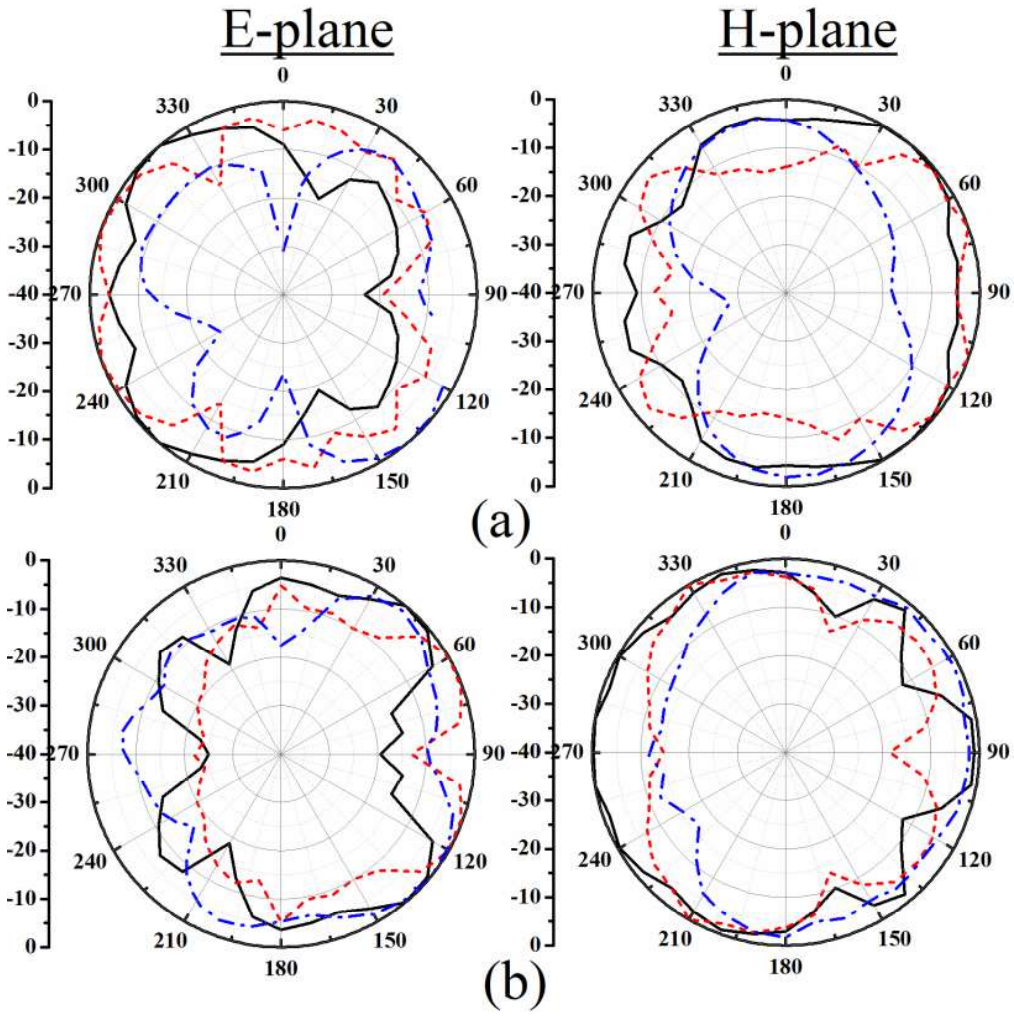

Figure 6.19: Radiation characteristics of the UWB MIMO antenna in E-plane and H-plane at 4.0 GHz (———), 6.4 GHz (- - - -) and 10.2 GHz (— • —) (a) port 1 is matched; (b) port 2 is matched

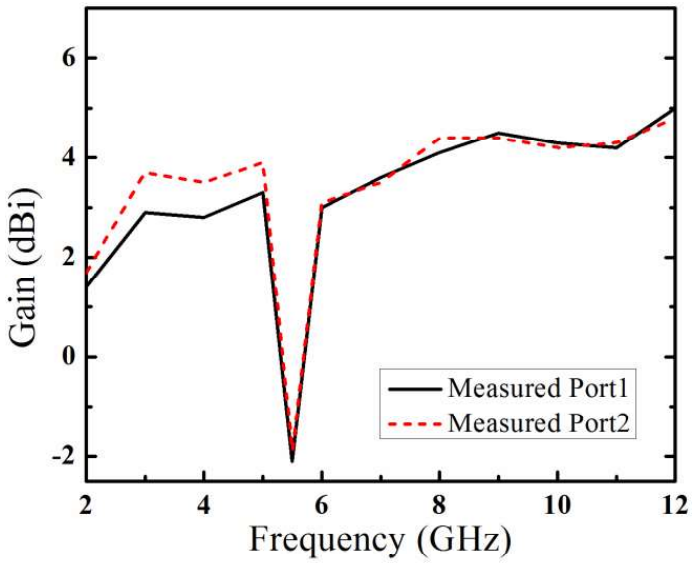

Figure 6.20: Measured gain of the proposed UWB MIMO antenna

(c) Diversity Performance

The ECC and capacity loss of the proposed fractal UWB MIMO antenna is shown in Figure 6.21. It is demonstrated from results that its value is less than 0.01 in the entire UWB band due to efficient design of the presented antenna, which is smaller than its threshold value 0.5 [Karaboikis *et al.*, 2008]. The quality of UWB MIMO system in a rich multipath environment is estimated in terms of capacity loss (b/s/Hz) to define the upper bound of rate of transmission for reliable transmission. In our case the capacity loss value is lower than 0.3b/s/Hz (mostly less than 0.2 b/s/Hz), except WLAN notch band, in the UWB operating range, which is lower than the threshold value 0.4 b/s/Hz.

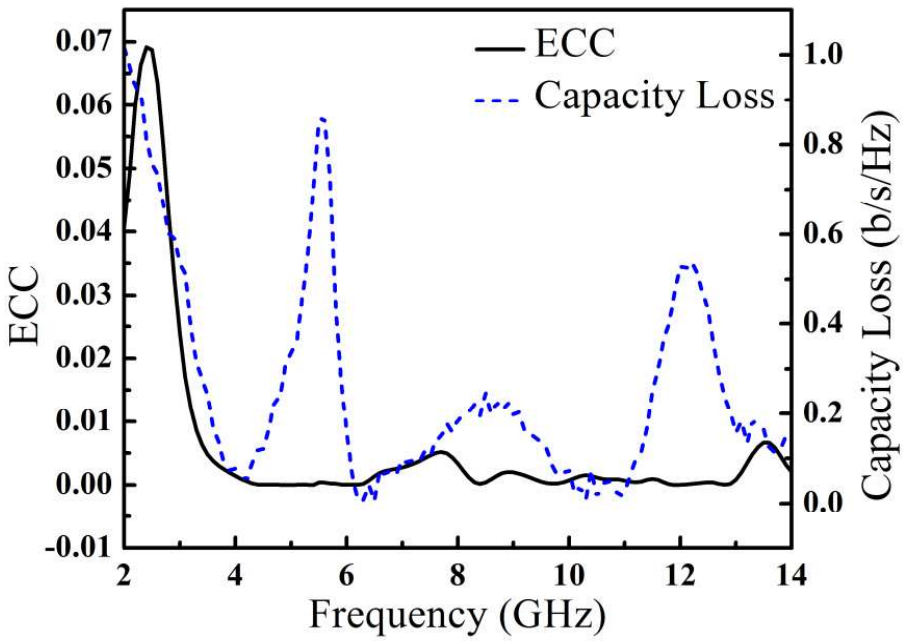

Figure 6.21: Capacity loss and ECC of the proposed fractal UWB MIMO antenna

6.4 Fractal Koch 2×2 UWB MIMO Antenna

6.4.1 Antenna Design

(a) Antenna Configuration

The geometry of the proposed 2×2 Koch fractal UWB MIMO antenna with WLAN band rejection is shown in Figure 6.22. It is fabricated on FR4 substrate (dielectric constant of 4.4, loss tangent of 0.02), with dimensions of 40 mm × 25 mm × 1.6 mm. The octagonal shaped fractal monopoles (FM) are placed orthogonal to each other, both fed by 50 Ω microstrip line. The orthogonal orientation of these two antenna elements helps to achieve better isolation between them [Karaboikis *et al.*, 2008]. The Koch fractal geometry is applied at the edges of octagonal shape monopole to achieve the desired miniaturization and wideband characteristics.

The generation of Koch fractal geometry and iteration wise evolution of single fractal monopole is described in section 3.7.1 (Figure 3.49 and 3.50). Here in the evolution of the monopole of the antenna, octagonal structure and Koch fractal work as initiator and generator, respectively. Furthermore, rectangular slots of dimensions L_{s2} × W_{s2} are introduced in the ground plane to achieve the UWB operational bandwidth. To obtain better isolation at lower frequency edge of UWB band, an L-shaped stub is extended from the ground plane between the two monopoles. It increases the effective current path and introduces an additional resonance at 2.6 GHz, which in turn improves isolation in UWB band. The band rejection in WLAN band is obtained by etching C-shaped slot from the FM of the UWB MIMO antenna. The analysis and design of the proposed UWB MIMO antenna is carried out using Ansoft HFSS ver.13. The optimized dimensions are as follows: L = 25 mm, W = 40 mm, R = 4.6 mm, W_m = 2.6 mm, L_g = 8.5 mm, T = 0.3 mm, d = 0.8 mm, L_1 = 1.2 mm, L_2 = 3.4 mm, L_3 = 7 mm, L_4 = 2.6 mm, L_5 = 15.5 mm, L_6 = 1 mm, L_7 = 6.25 mm, W_1 = 6.2 mm, W_2 = 9.2 mm, L_{s1} = 3.5 mm, W_{s1} = 1 mm, L_{s2} = 1.5 mm, W_{s2} = 5 mm, L_{s3} = 1 mm, W_{s3} = 1.5 mm, L_{s4} = 2 mm, W_{s4} = 8 mm, L_{s5} = 1 mm, and W_{s5} = 2 mm.

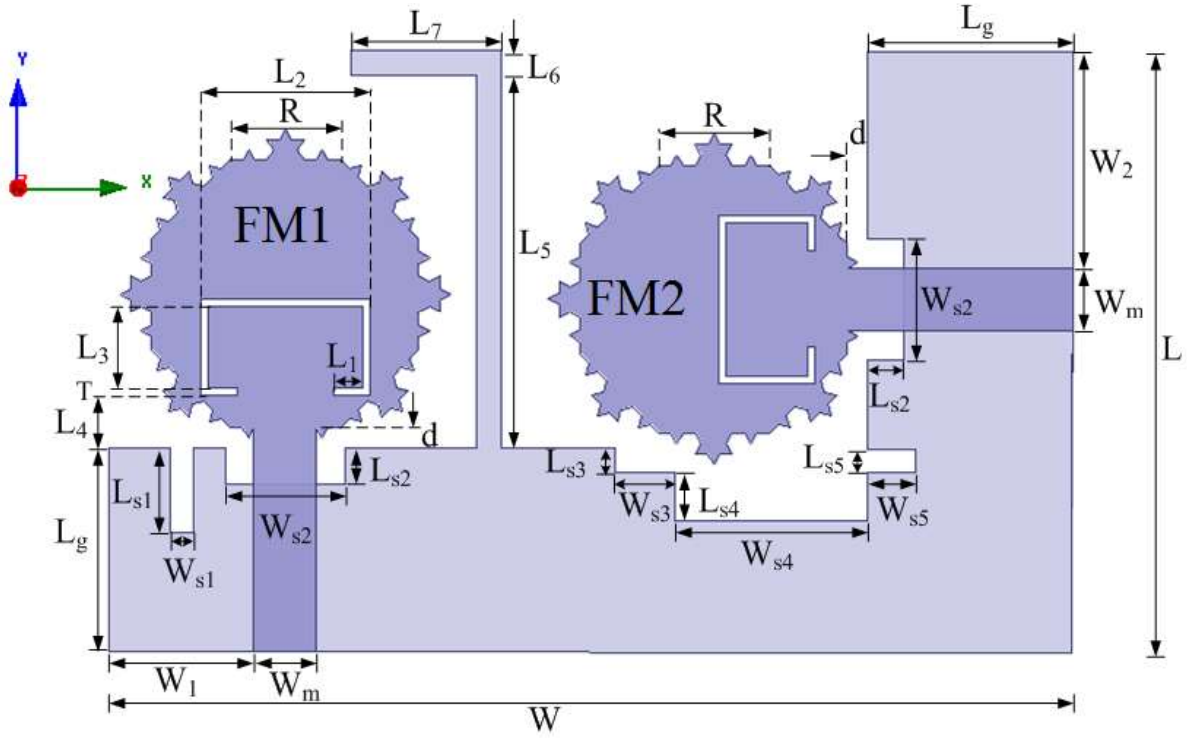

Figure 6.22: Geometry of the proposed fractal UWB MIMO antenna

(b) Effect of L-shaped ground stub

Figure 6.23 shows the effect of L-shaped stub on the S-parameters of the antenna. It is observed from Figure 6.23(a) that the impedance bandwidth S_{11}<-10 dB improves significantly at lower and higher frequencies in the UWB operating band after the introduction of L-shaped ground stub, which helps to obtain the operating bandwidth from 3.3-10.8 GHz with three resonant frequencies at 4, 6.4, and 9.6 GHz, whereas impedance bandwidth response of S_{22}<-10 dB improves at higher frequencies. These improvements can be attributed due to increment in the surface current path. It is noticed that isolation of more than 15dB is required in UWB MIMO antenna for good performance [Zhang *et al.*, 2009; Peng *et al.*, 2014]. It is observed from Figure 6.23(b) that the decoupling bandwidth response is suppressed significantly at lower frequency after the introduction of L-shape ground stub, which in turn helps to achieve decoupling bandwidth from 2.4-14 GHz.

The effect of L-shaped ground stub can be expressed in terms of the surface current distributions of UWB MIMO antenna at 4 GHz and 9.6 GHz resonant frequencies. It is observed from Figure 6.24(a) and (b), when port 1 is excited, that at 4 GHz resonant frequency significant amount of surface current is coupled to the ground stub, which leads to the reduction of surface currents at FM2 of the antenna from FM1. Thus, increment in impedance bandwidth and decoupling bandwidth at low frequency is also observed. When port 2 is excited at 4 GHz, Figure 6.24(c) and (d) shows that significant amount of current is coupled to the stub and flow of surface current from FM2 to FM1 is reduced significantly. Figure 6.24(e) and (f) shows that, at 9.6 GHz, when port 1 is excited, the surface current intensity at both the FMs increases as compared to lower resonant frequency, which leads to improvement in S_{11} and S_{21} in the UWB spectrum as well as radiation characteristics of the antenna. Similarly, for Figure 6.24(g) and (h) when port 2 is excited, at 9.6 GHz, stub blocks the flow of currents from FM2 to FM1 when compared to the case without the stub and with the stub.

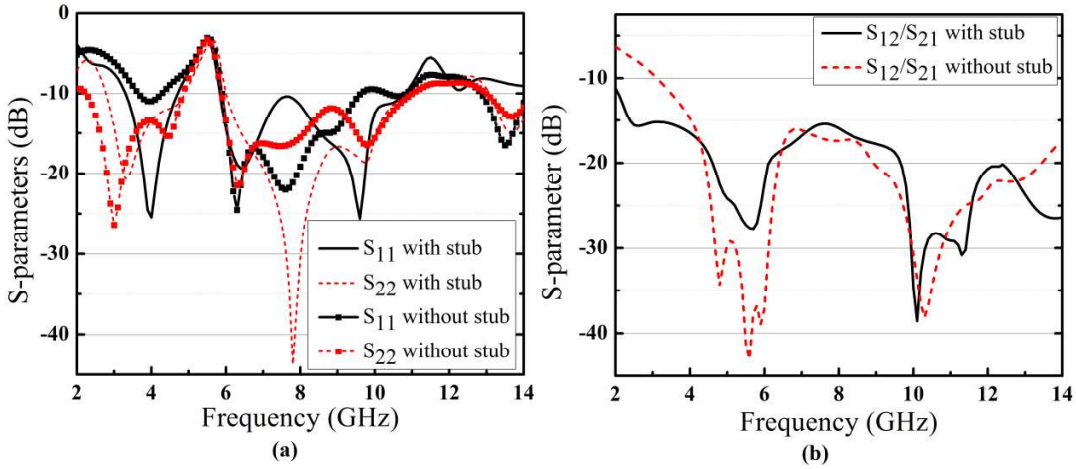

Figure 6.23: Simulated S-parameters variation of proposed fractal UWB MIMO antenna with and without ground stub (a) S_{11} and S_{22}, (b) S_{21} and S_{12}

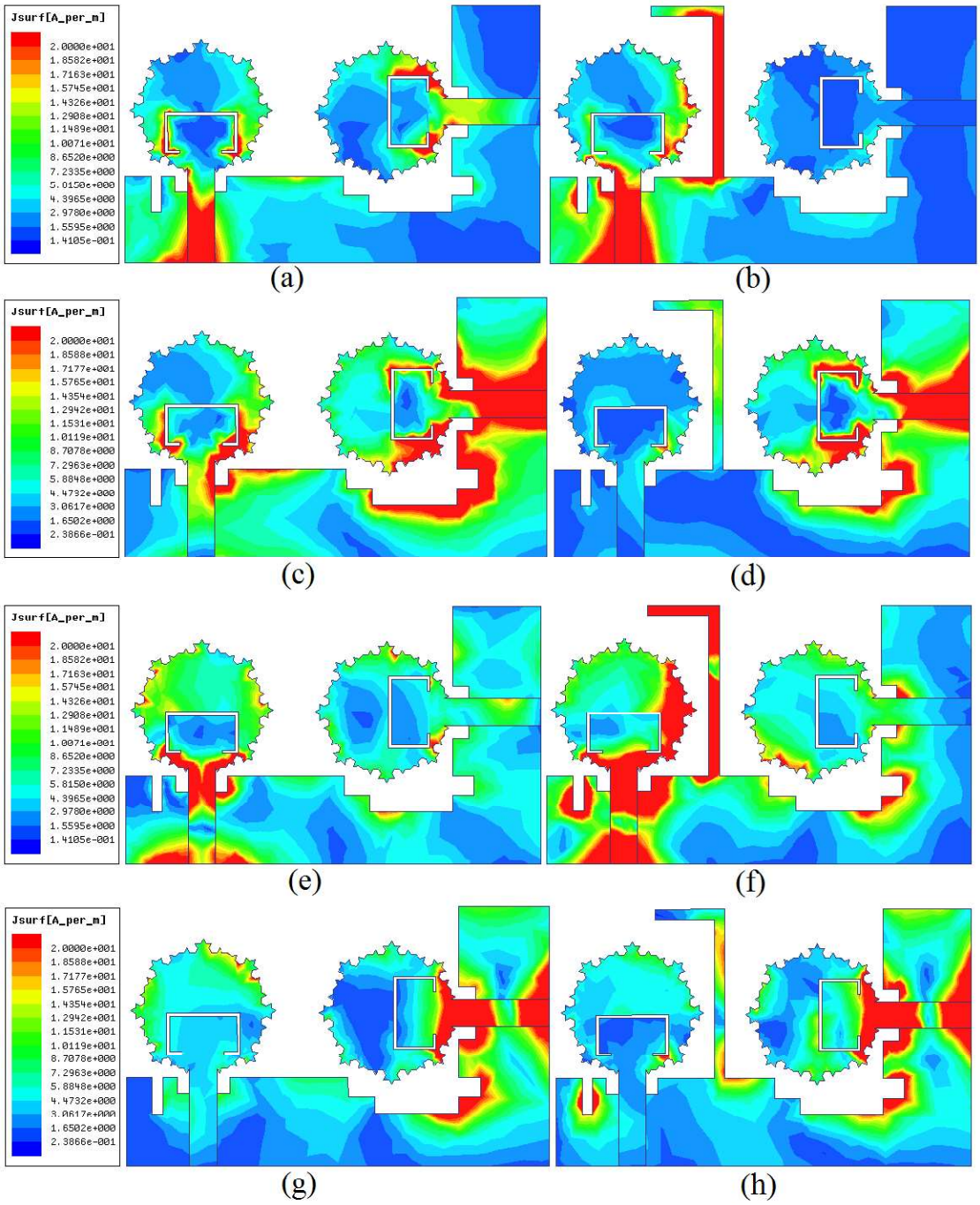

Figure 6.24: Simulated surface current distribution (a) at 4 GHz without L-shape stub when port1 is excited, (b) at 4 GHz with L-shape stub when port1 is excited, (c) at 4 GHz without L-shape stub when port2 is excited, (d) at 4 GHz with L-shape stub when port2 is excited, (e) at 9.6 GHz without L-shape stub when port1 is excited, (f) at 9.6 GHz with L-shape stub when port1 is excited, (g) at 9.6 GHz without L-shape stub when port2 is excited and (h) at 9.6 GHz with L-shape stub when port2 is excited

(c) Effect of C-shaped slot

The band rejection characteristics over the WLAN (5.15-5.825 GHz) notch band is obtained by etching C-shaped slot from the fractal monopole of the antenna. The length of the slot is calculated mathematically by the following expression:

$$L = \frac{c}{2f_{notch}\sqrt{\varepsilon_{eff}}} \approx 2L_1 + L_2 + 2L_3 \tag{6.6}$$

where, c is speed of the light, ε_{eff} is the effective dielectric constant, and L is the length of the slot. The calculated length of the C-shaped slot using Eq. (6.6) is 16.2 mm, whereas actual length is 16.6 mm, which is close to calculated length. It can be observed from simulated surface current distribution of antenna at 5.5 GHz notch frequency in Figure 6.25 that when port1/port2 is excited, the surface current is concentrated near the C-shaped slot only.

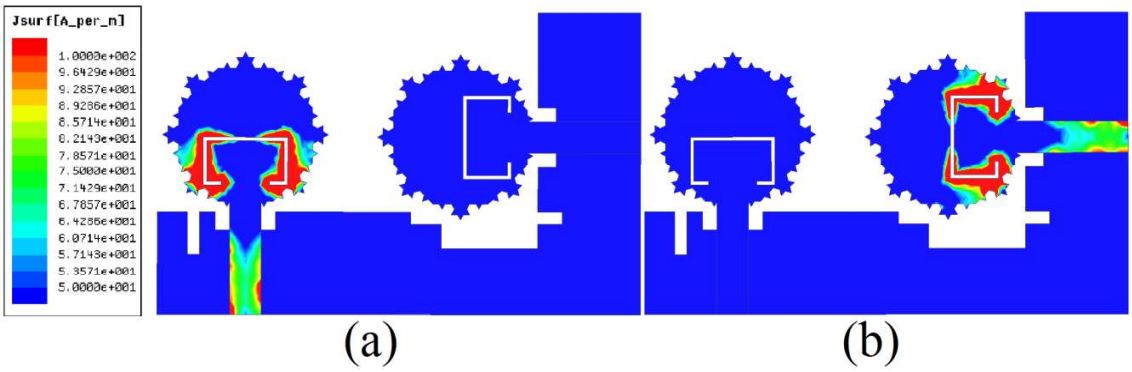

Figure 6.25: Simulated surface current distribution at 5.5 GHz notch frequency (a) port 1 is excited and (b) port 2 is excited

6.4.2 Results and Discussion

(a) S-parameter Result

To verify the concept of presented UWB MIMO antenna, the prototype of the antenna is fabricated and is measured using Agilent E5071C vector network analyzer (VNA). The photographs of the fabricated UWB antenna with its top and bottom view are shown in Figure 6.26. The simulated and measured S_{11}, S_{22} and S_{21} of the UWB MIMO antenna are shown in Figure 6.27.The measured S_{11} and S_{22} results are in good agreement with simulated results. The mutual coupling behavior of antenna is less than -15 dB. Thus, the presented UWB MIMO antenna satisfies the desired characteristics in the UWB operating range, so the antenna is an appropriate choice for portable UWB MIMO system.

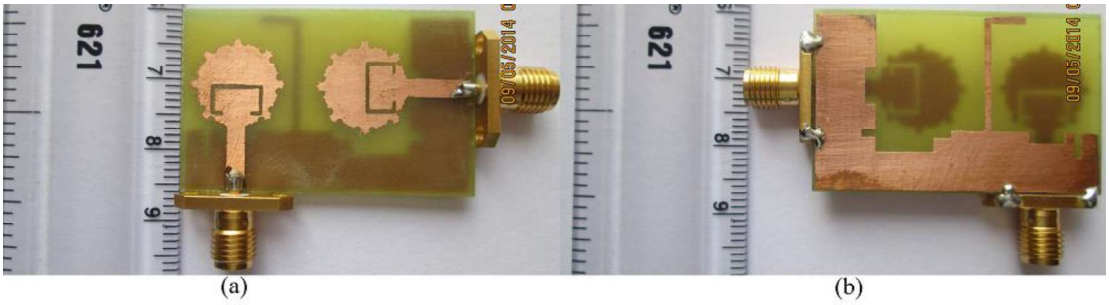

Figure 6.26: Photograph of the fabricated UWB MIMO antenna (a) front view and (b) rear view

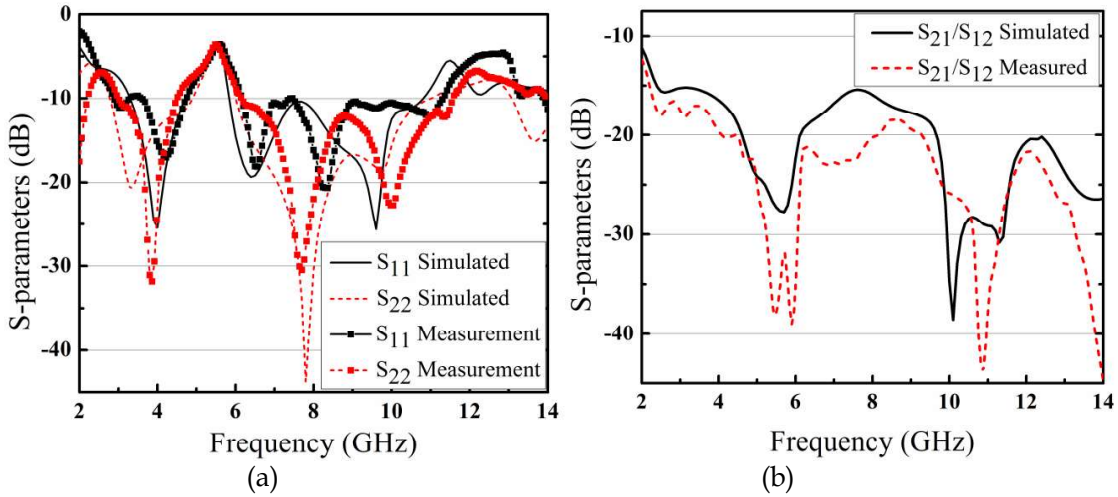

Figure 6.27: Comparison of simulated and measured S-parameters result (a) S_{11} and S_{22} and (b) S_{21} and S_{12}

(b) Radiation Performance

Figure 6.28 shows the measured gain of the proposed antenna for both ports in the UWB band. The gain response is within 3dB variation range outside WLAN notch band. The gain response is suppressed significantly in the notch band. Figure 6.29 shows the measured radiation pattern in E-plane (*xz*-plane) and H-plane (*yz*-plane) at different resonant frequencies. It is observed that radiation pattern is quasi- omnidirectional in H-plane. Figure 6.28(a) shows the radiation pattern at resonant frequencies when port 1 is excited, whereas port 2 is terminated using a 50 Ω matched load. Figure 6.28(b) displays the radiation pattern when port 2 is excited and port 1 is terminated with a 50 Ω matched load. The radiation pattern at higher frequencies shows small distortion compared to lower frequencies due to the reflection at edges from the fractal monopole of antenna. The bends and curves of fractal geometry cause for the change in current path, which in turn leads to enhancement in radiation characteristics of the antenna [Balanis, 2005].

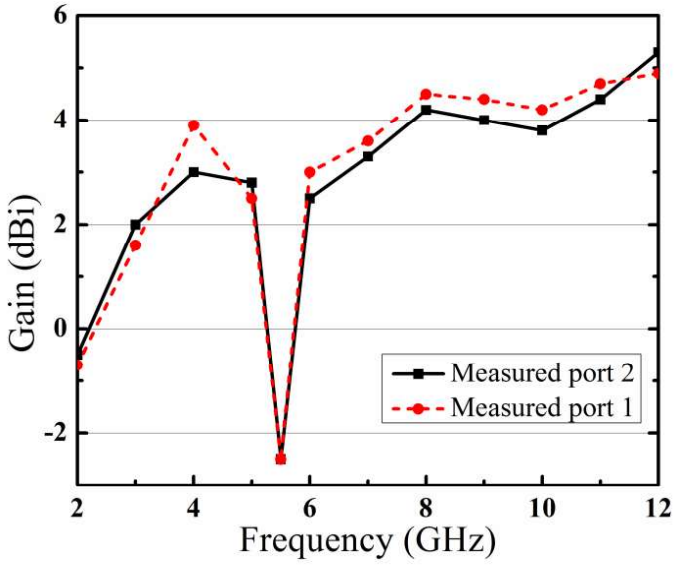

Figure 6.28: Measured gain of the proposed UWB MIMO antenna

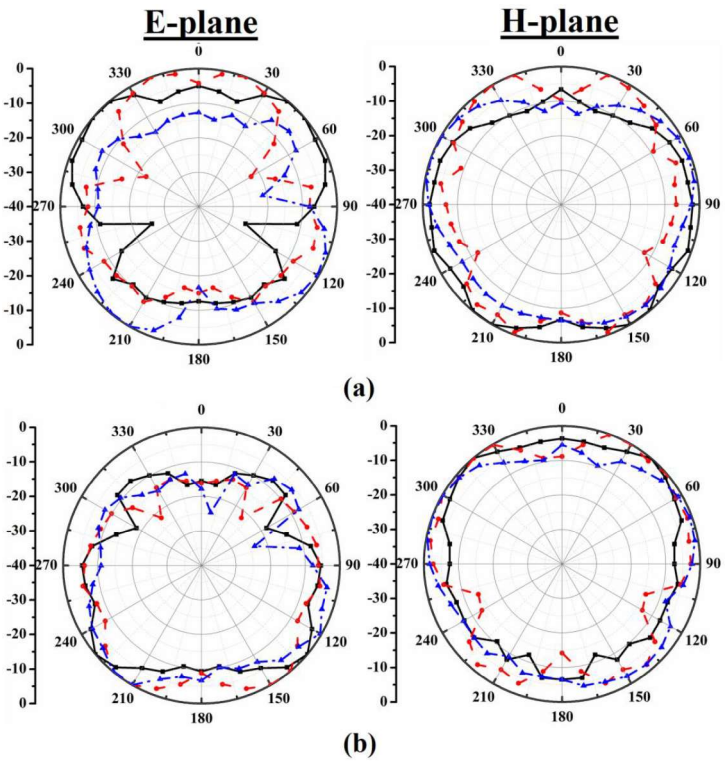

Figure 6.29: Radiation characteristics of the UWB MIMO antenna in E-plane and H-plane at 4.0 GHz (——), 6.4 GHz (– –) and 9.6 GHz (—·—·—) (a) port 1 is matched and (b) port 2 is matched

(c) Diversity Performance

Figure 6.30 represents the ECC of the proposed UWB MIMO antenna. It is observed that ECC value is less than 0.01 across the entire UWB range due to its efficient design, whereas for good diversity performance its value should be less than 0.5 [Karaboikis *et al.*, 2008]. This indicates that the good diversity performance is achieved by the proposed UWB MIMO antenna.

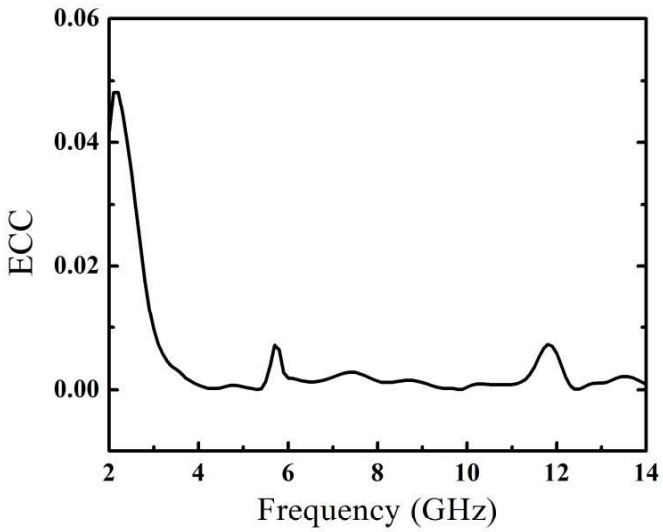

Figure6.30: ECC of the proposed UWB MIMO antenna

Figure 6.31 shows the capacity loss changes with the variation of frequencies. It is observed that the capacity loss value are always less than 0.3 b/s/Hz in the UWB operating range, except for WLAN notch band, where it is higher than the threshold value of 0.4 b/s/Hz.

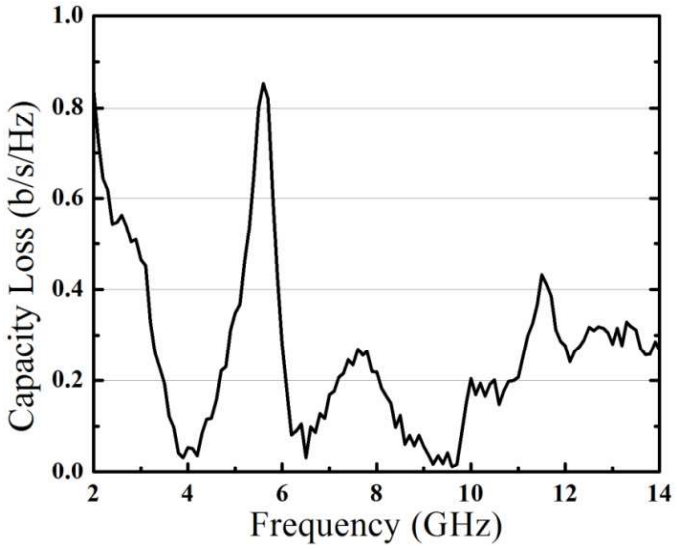

Figure 6.31: Capacity Loss of the proposed UWB MIMO antenna

6.5 Fractal Koch 4×4 UWB MIMO Antenna

6.5.1 Antenna Design

(a) Antenna Configuration

In the last section of the chapter, 4×4 fractal UWB MIMO antenna (FUMA) as shown in Figure 6.32 is presented and its characteristics are investigated. In the design process, Koch fractal geometry is applied at the edges of octagonal geometry. It shows wide operational bandwidth with desired radiation characteristics. The generation of Koch fractal geometry and iteration wise evolution of single fractal monopole is described in section 3.7.1 (Figure 3.49 and 3.50). Here, the octagonal shape work as an initiator and Koch geometry work as a generator in the evolution of FM of the antenna. Moreover, rectangular slots are introduced in the ground plane to improve the impedance matching. It can be seen that the optimal design of the antenna provide operational bandwidth in the desired UWB band as well as satisfactory radiation characteristics. The presented antenna shows mutual coupling less than -17 dB in the operating range from 2-10.6 GHz, which cover entire UWB operational range. Moreover, further enhancement in isolation is achieved by placing a grounded stub among the antenna monopoles. In order to achieve the notch band characteristics in WLAN band, a C-shaped slot is etched from the FM. The optimized antenna geometry is fabricated on FR4 substrate with dimension of 45 mm × 45 mm × 1.6 mm, dielectric constant of 4.4, and loss tangent of 0.02. The MIMO system consists of four FMs, each one is fed by a microstrip line of 50 Ω. The ground plane is placed on the other side of the substrate. The orthogonal orientation of adjacent antenna elements helps to achieve better isolation among them [Karaboikis *et al.*, 2008]. A rectangular slot of dimensions $L_s \times W_s$ is introduced in the ground plane below the feed line, which in turn leads to increase the current path and helps to achieve the desired UWB band. To reduce the mutual coupling rectangular grounded stubs are placed among antenna elements, which act as a reflector.

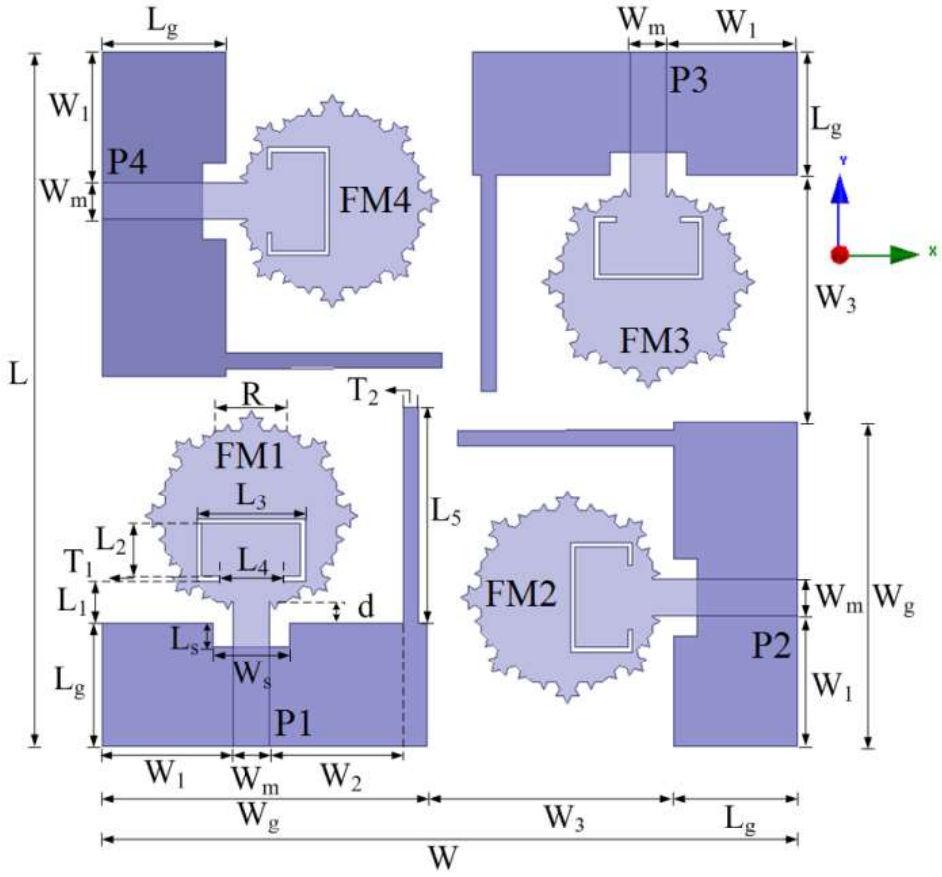

Figure 6.32: The optimized geometry of the proposed 4×4 FUMA

In addition, a C-shaped slot is etched from FMs to provide the band notch characteristics in WLAN band. The optimization and designing of proposed FUMA is carried out using HFSS v.13. The optimized dimensions are: L = 45 mm, W = 45 mm, R = 4.6 mm, W_m = 2.3 mm, L_g = 8 mm, W_g = 21 mm, T_1 = 0.3 mm, T_2 = 1 mm, d = 1.3 mm, L_1 = 2.7 mm, L_2 = 3.4 mm, L_3 = 7 mm, L_4 = 4 mm, L_5 = 14 mm, W_1 = 6.2 mm, W_2 = 9.2 mm, W_2 = 9.2 mm, L_s = 3.5 mm, and W_s = 1 mm.

(b) Effect of grounded stubs

The proposed FUMA is composed of four FMs, there is strong mutual coupling among the antenna elements when they are close to each other, which in turn leads to poor isolation of 12 dB at the edges of UWB band. Hence, the grounded stubs are introduced in the geometry to enhance the isolation. Thus, to get more insight into the effect of grounded stubs, with and without in terms of S-parameters variation, are carried out as shown in Figure 6.33. It is observed from Figure 6.33(a) that ground stub helps to improves operating bandwidth at low and high frequency significantly due to increment in the current path. Besides, the isolation of more than 15 dB is required for good antenna performance [Zhang *et al.*, 2009; Peng *et al.*, 2014]. Figure 6.33(b) shows that all three parameters S_{21}, S_{31} and S_{41} isolation responses are better than 17 dB after introduction of stub in the geometry.

Figure 6.34 shows that the simulated current distribution with and without ground stub at 3.9 GHz resonant frequency to further study the behavior of the FUMA. When port 1 is excited and other ports 2, 3 and 4 are terminated with 50 Ω load, it is observed that flow of current from port 1 to other port is reduced significantly, because stub work as a reflector and prevent the coupling of electromagnetic energy among FMs. However, due to symmetry only port 1 response is shown and other port response is omitted.

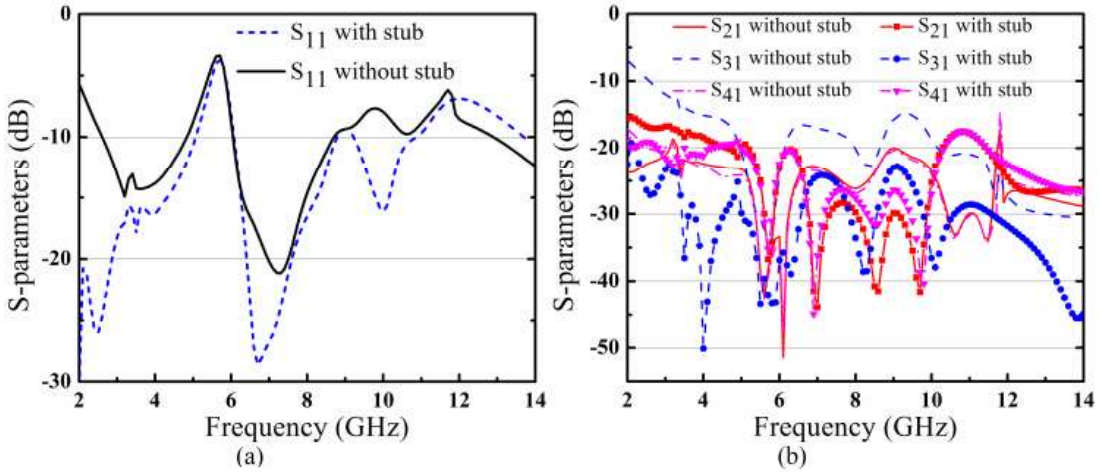

Figure 6.33: Simulated S-parameters variation of proposed fractal UWB MIMO antenna (a) S_{11} with and without ground stub and (b) S_{21}, S_{31}, S_{41} with and without ground stub

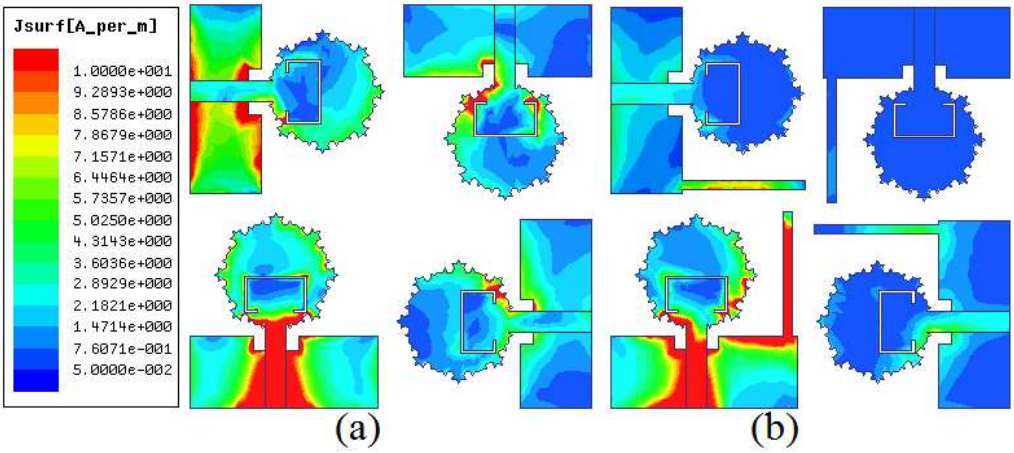

Figure 6.34: Simulated surface current distribution at 3.9 GHz when port 1 is excited (a) without stub and (b) with stub

(c) Effect of C-shaped slot

The band rejection characteristics at WLAN (5.15-5.85 GHz) band is achieved by etching C-shaped slots from FMs. The length of the slot is estimated by mathematical formula:

$$L_n = \frac{c}{2f_{notch}\sqrt{\varepsilon_{eff}}} \approx 2L_2 + 2L_3 - L_4 \tag{6.8}$$

where, c is speed of light, ε_{eff} is the effective dielectric constant as calculated in [Pozar, 1998], L_n is the length of the slot, and L_2, L_3 and L_4 are design parameters. The calculated length of the slot using (1) is 16.2 mm, whereas actual length of slot is 16.8 mm, it is very close to the calculated length. The simulated surface current distribution of antenna at notch frequency is shown in Figure 6.35. As it can be seen, that the current intensity is higher at the inner and the outer edges of C-shaped slot in FM compared to other parts of the FM. This leads to high suppression of radiation characteristics at the notch frequency, which in turn reduces the gain of the antenna at WLAN notch band.

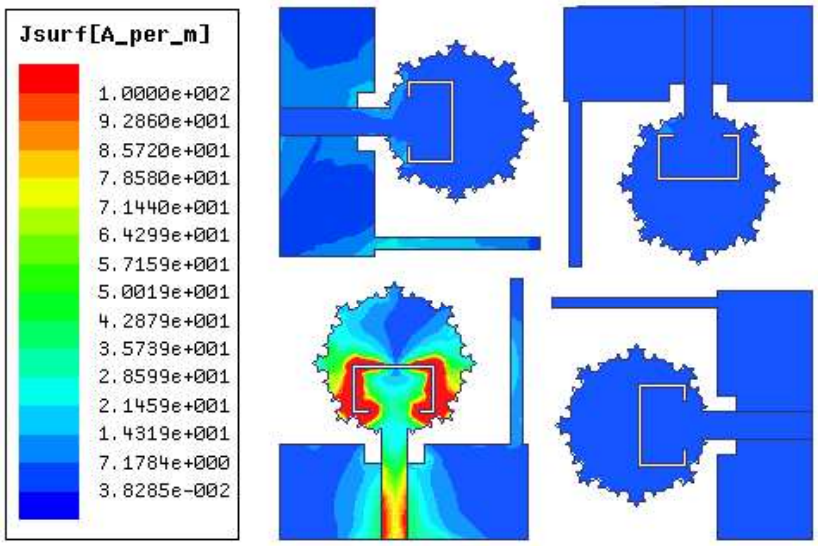

Figure 6.35: Simulated surface current distribution at 5.5 GHz notch frequency with port 1 excited and port 2, 3 and 4 terminated

6.5.2 Results and Discussion

(a) S-parameter Result

The proposed FUMA is fabricated and its bandwidth performance is measured by using Agilent E5071C vector network analyzer (VNA). Figure 6.36 shows the fabricated photograph of the FUMA. The simulated and measured S-parameters of the antenna are represented in Figure 6.37. The simulated and measured results of only S_{11}, S_{21}, S_{31} and S_{41} are discussed because of symmetrical arrangement of antenna elements in the structure. It is seen from Figure 6.37(a) that, the measured operating bandwidth is from 3-10.6 GHz excluding 5.5 GHz notch band. However, some discrepancies are observed because of fabrication tolerances, soldering and losses due to SMA connectors. Figure 6.37(b) shows that the mutual coupling is below -19 dB for most of the band excluding lower and higher operating edges of UWB band, where its value is -17 dB. The measured results are in good agreement with simulated one.

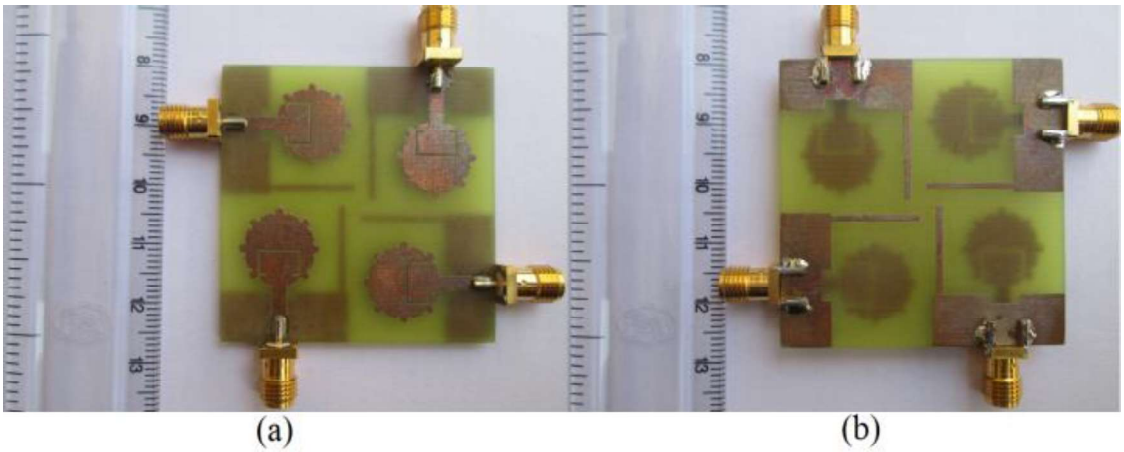

Figure 6.36: Photograph of the fabricated UWB MIMO antenna (a) front view, and (b) rear view

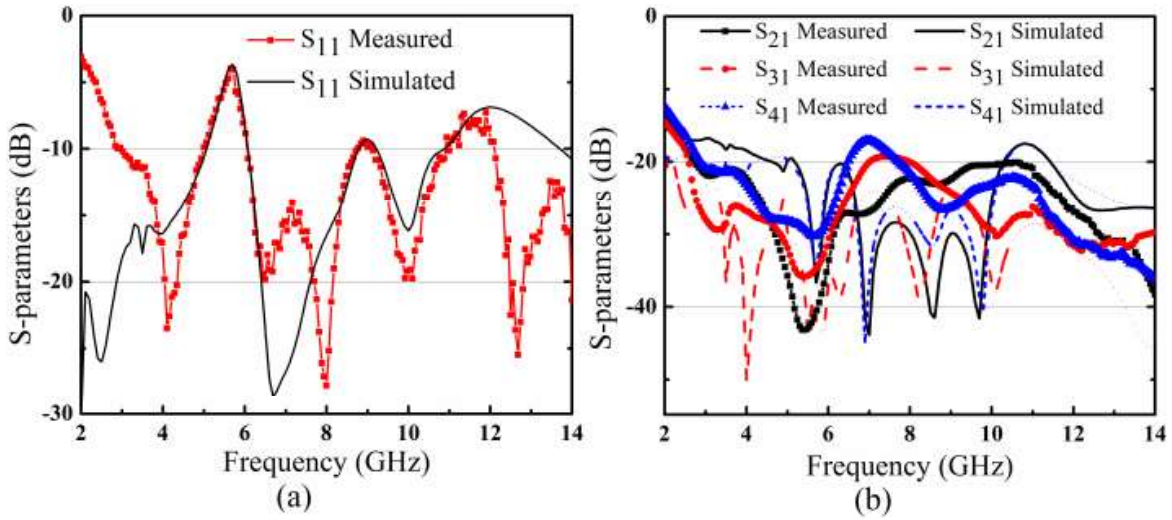

Figure 6.37: Comparison of simulated and measured S-parameters result (a) S_{11} and (b) S_{12}, S_{13}, and S_{14}

(b) Radiation Performance

Figure 6.38 shows the measured radiation pattern of FUMA at 3.9, 6.7 and 10 GHz resonant frequencies, when port 1 is excited and other ports 2, 3 and 4 are terminated by a 50 Ω load. It can be observed that radiation pattern in E-plane (*xz*-plane) is directed more towards –y directions, whereas in H-plane (*yz*-plane) is quasi-omnidirectional. Moreover, bends and curves of Koch fractal geometry cause for the change in current path, which helps to enhance the radiation characteristics of the antenna [Pozar, 1998]. This enhancement in radiation characteristics helps to improve the gain of the antenna. Figure 6.39 shows the measured gain of the proposed FUMA. The gain response is within 3dB variation range excluding WLAN notch band, when port 1 (P1) is excited and other ports are matched to 50Ω loads. Furthermore, a significant reduction in gain response is observed in the notch band.

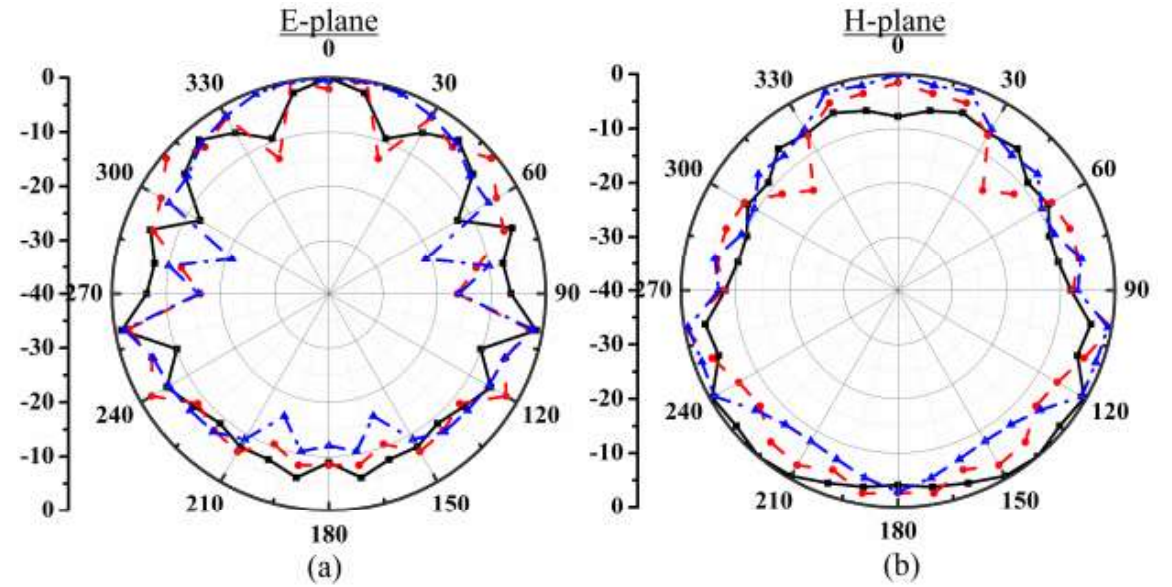

Figure 6.38: Radiation characteristics of the UWB MIMO antenna in E-plane and H-plane at 3.9 GHz (——), 6.7 GHz (– –) and 10 GHz (—·—) when port 1 is excited and other ports are terminated

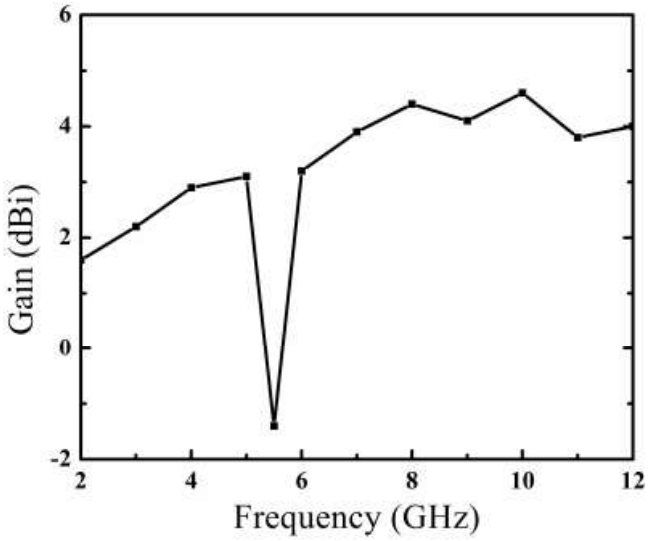

Figure 6.39: Measured gain of the proposed UWB MIMO antenna

(c) Diversity Performance

Normally, the value of ECC, less than 0.5 represents accepted threshold level of signal distortion [Koohestani *et al.*, 2014]. The ECC value of proposed FUMA is below 0.005 across the entire UWB operating band due to effectiveness of the presented FUMA. Similarly, in a rich multipath environment capacity loss (b/s/Hz) is estimated to define the upper bound of rate of transmission for reliable transmission in a communication channel. In case of a 4×4 MIMO antenna its accepted value should be less than 0.4 b/s/Hz [Li *et al.*, 2012; Choukiker *et al.*, 2014]. Figure 6.40 shows the capacity loss changes with the variation of frequencies. It can be seen that the capacity loss values are always smaller than 0.3 b/s/Hz in the UWB operating range, except for WLAN notch band, where it is more than the threshold value of 0.4 b/s/Hz.

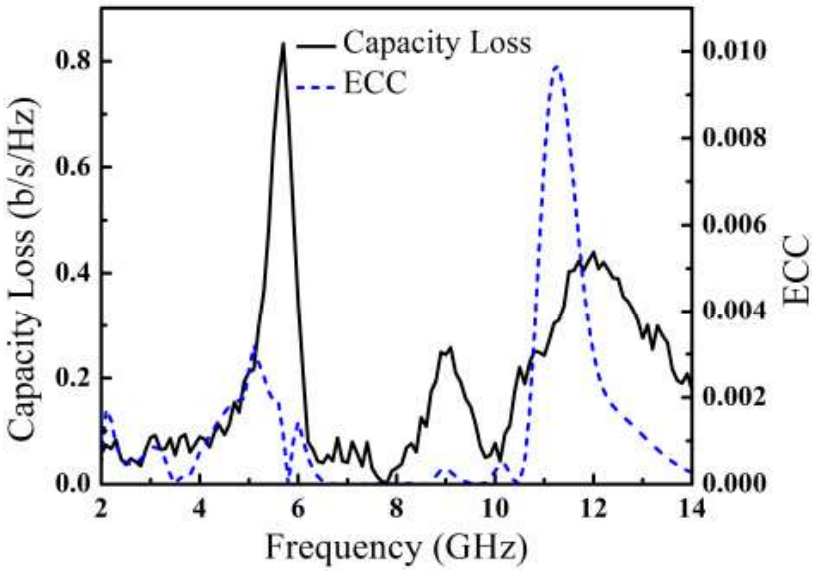

Figure 6.40 Capacity loss and ECC of the proposed FUMA

Table 6.1: Comparison of the proposed work with others presented in the literature

Antenna	Dimensions (mm×mm×mm)	Bandwidth (GHz)	Band-notch Band (GHz)	Isolation (dB)	Capacity Loss(b/s/Hz)
Work in Section 6.2	25×35×1.6	2.6-13.5	5.15-5.85	>16	< 0.3
Work in Section 6.3	25×40×1.6	3.3-10.7	5.15-5.85	>15	<0.3
Work in Section 6.4	25×40×1.6	3.3-10.8	5.15-5.85	>15	<0.3
Work in Section 6.5	45×45×1.6	2-10.6	5.15-5.85	>17	<0.3
Li *et al.*, 2013	30×27×0.8	3.1-10.6	5.15-5.85	>20	-
Peng *et al.*, 2014	48×48×0.8	2.9-12	5.15-5.85	>15	-
Lee *et al.*, 2012	86.5×55×0.8	1.8-10.6	-	>14.8	-
Kiem *et al.*, 2014	60×60×1.6	2.98-11.2	5.15-5.85	>15	-

6.6 Summary

The application of fractal geometry in the UWB MIMO antenna design is investigated in this chapter. It is demonstrated that the fractal geometry helps to achieve desired miniaturization and wide operational bandwidth due to its self-similar and space filling properties. It has been shown that the bends and curves of fractal geometry causes for the change in current path, which in turn leads to enhance the radiation characteristics of the antenna. The Minkowski fractal geometry is applied as a fractal slot in the ground plane in first antenna design and applied at the edges of octagonal shape monopole in the second antenna design. In both the cases, it helps to achieve stable radiation pattern. The Koch fractal geometry is used in the third and fourth antenna design for 2×2 and 4×4 UWB MIMO antenna design, respectively. It is demonstrated that these antennas also shows an ultra-wide operational bandwidth with reasonable radiation pattern. Capacity loss is smaller in a 4×4 fractal UWB MIMO compared to a 2×2 fractal UWB MIMO antenna. In order to achieve the band rejection in the WLAN band elliptical and C-shaped slots are introduced in the monopoles of the antenna. Moreover, a ground stub is placed among the antenna elements to improve the isolation in a smaller area, which helps to achieve the compactness in the design and enhances the radiation characteristics of the antenna, too. Table 6.1 shows, a comparative study among different UWB MIMO antennas, presented in the chapter as well as other work available in the literature, is provided in terms of dimension, bandwidth, notch-band, isolation and capacity loss. Thus, it can be concluded form results that the presented 2×2 and 4×4 fractal MIMO antennas are good candidates for portable UWB applications.

…